Timing and patterns of ENSO impacts in Africa over the last 30 years: insights from Normalized Difference Vegetation Index data.

Nathalie Philippon, Aurélie Blais, Nadège Martiny, Pierre Camberlin, Timm Hoffman

Elsevier Editorial System(tm) for Remote Sensing of Environment
Manuscript Draft

Manuscript Number:

Title: Timing and patterns of ENSO impacts in Africa over the last 30 years: insights from Normalized Difference Vegetation Index data.

Article Type: Full length article

Keywords: ENSO; Africa; Normalized Difference Vegetation Index; teleconnection patterns

Corresponding Author: Dr. Nathalie Philippon,

Corresponding Author's Institution: Centre de Recherches de Climatologie

First Author: nathalie philippon, Dr

Order of Authors: nathalie philippon, Dr; Aurélie Blais, MsC; nadège martiny, Dr; pierre camberlin, Pr; Timm Hoffman, Pr

highlights

- the ENSO impact in Africa is evaluated at a monthly time-step using NDVI
- along the seasonal cycle, several dipolar and propagative patterns appear
- significant signals are observed over the less-studied winter rainfall regions

*Manuscript

Timing and patterns of ENSO impacts in Africa over the last 30 years: insights from Normalized Difference Vegetation Index data.

Submitted to Remote Sensing of Environment

February 2012

Philippon N°[1], Blais A[1], Martiny N[1], Camberlin P[1], Hoffman M.T[2]

° nphilipp@u-bourgogne.fr

tel: 0033 3 80 39 38 21, fax: 0033 3 80 39 57 41

[1] Centre de Recherches de Climatologie, Biogeosciences UMR5561 CNRS / Université de Bourgogne, 6 blvd Gabriel, 21000 Dijon, France

[2] Plant Conservation Unit, Botany Department, University of Cape Town, Private Bag X3, Rondebosch, 7701, South Africa.

Abstract

In this study we reassess and provide a more complete picture of the timing and patterns of ENSO impacts for the whole of Africa over the three last decades. We analyse the vegetation photosynthetic activity estimated by the NOAA-AVHRR Normalized Difference Vegetation Index (NDVI) rather than rainfall itself, because NDVI allows us to document the impacts at fine space and time scales. The use of the monthly time-step adds important new insights to the findings of previous works based largely on annual or seasonal time-scales and on a regional spatial-scale: several dipolar and propagative patterns are highlighted. In addition, we show that the less-studied winter rainfall regions at the southwestern and northwestern tips of the continent are impacted as well. Starting from July (the beginning of the peak phase of ENSO), to June (the post phase of ENSO), the teleconnection patterns over the whole of Africa evolve as follows. From July to September, negative correlations between NDVI and N3.4 are observed north of the equator but they are not uniform in space and are moderate (~0.3) except towards the east. Conversely, positive correlations are recorded over the winter rainfall region of South Africa. In the period from October-November, two dipoles develop: a north/south one in West Africa signaling a latitudinal modulation of the ITCZ location, and a west/east one in East Africa signaling a longitudinal modulation of the ITCZ location. By December (end of the peak phase of ENSO), with the settlement of the ITCZ south of the equator, positive correlations over the Horn of Africa spread southward and westward while negative correlations appear over Mozambique, Zimbabwe and South Africa. This pattern strengthens and a dipole at 18°S is well established in January-March (the decay phase of ENSO). In the meantime, by ~2°N negative correlations spread northward, while at the northwestern tip of Africa, a west/east dipole occurs opposing Algeria and eastern Morocco (positive correlations) with western Morocco (negative correlations). Lastly, at the end of the ENSO decay phase and the beginning of its post phase (April 1 to June 1) a northward (to 10°S) and eastward (to the south of Tanzania) spread of the negative correlations south of 18°S occurs

while the positive correlations over equatorial East Africa switch to being negative.

1/ Introduction:

The El Niño / La Niña Southern Oscillation (ENSO/LNSO) is the main mode of climate variability at the global scale. During ENSO/LNSO events, the atmospheric circulation and precipitation patterns are strongly disturbed for several months worldwide and more particularly in the tropics (e.g. Dai and Wigley 2000). For that reason, the predictability and prediction of ENSO/LNSO events have long been considered (Latif et al 1998, Chen et al 2004) and forecasts based either on numerical and statistical models or a combination of the two are now routinely performed. Given the relatively predictable nature of ENSO/LNSO an accurate understanding of its timing and pattern of impact should help to mitigate its effects in different parts of the world. Because of Africa's economic (e.g. the importance of primary production, endemic poverty) and social (e.g. rapidly growing population, low Human Development Index, poor governance, armed conflicts) characteristics, it is highly vulnerable to climate variability and change (Thornton et al 2006). The teleconnections between ENSO and African rainfall have been the subject of numerous studies. However, most of them are performed at seasonal to annual time scales and usually focus on specific regions within Africa, rarely on the continent as a whole (e.g. Nicholson and Kim 1997). Therefore, neither the precise timing of the impact of ENSO nor the patterns (e.g. propagations, dipoles) have been fully documented. In addition, while the impacts of ENSO in the summer rainfall areas and semi-arid tropics (Sahel, Southern Africa, Horn of Africa) are regularly investigated (e.g. Segele et al 2008, Fauchereau et al 2009, Crétat et al 2010, Fontaine et al 2011, Mohino et al 2011, among many others), the humid to sub-humid regions and those experiencing winter rainfall (at the northwest and southwest tips of the continent) have drawn less attention (see Knippertz et al 2003, Balas et al 2007, Philippon et al 2011). However, several of these regions are densely populated and are net exporters of high quality agricultural products. This calls for a better knowledge of their climate variability, particularly as it relates to ENSO.

Furthermore, most of the studies performed on the African rainfall / ENSO teleconnections consider long time periods (usually 50 years from the 1950's). However, these teleconnections are subject to a strong decadal variability, and for many regions in Africa, they have become much more intense since the end of the 1970's (e.g. Janicot et al 1996, Richard et al 2000, Knippertz et al 2003, Philippon et al 2011). In parallel, however, since the end of the 1970's, in-situ rainfall data in Africa have become more and more scarce (e.g. the number of rain-gauges used in the Global Precipitation Climatology Center rainfall database has decreased from 4196 in the early 1980's to 1536 in the late 2000's, Rudolf et al 2010) and less reliable. Unfortunately, rainfall estimates from satellites still do not adequately capture the climatology and variability in rainfall over the continent and its sub-regions, and feature important biases in rainfall patterns and quantities (Nicholson et al 2003, Ali et al 2005, Dinku et al 2007, McCollum et al 2000). High-resolution products are also not available for a sufficiently long period of time to enable a consistent and precise mapping of the ENSO impact on local climate conditions.

Thus, the objective of this study is to reassess and provide a more complete picture of the timing and patterns of ENSO impacts in the whole of Africa over the three last decades. To circumvent the issue of in-situ rainfall data scarcity and reliability over the last decades, and to document ENSO impacts at fine space and time scales, we have analyzed the vegetation photosynthetic activity estimated by the Normalized Difference Vegetation Index (NDVI), rather than rainfall itself. The frequent and regular update of the database, the 8km spatial resolution over the whole of Africa, and the 10-day time resolution are among the advantages of using NDVI over rainfall. This also provides the opportunity to assess the sensitivity of vegetation photosynthetic activity to rainfall variability over the whole of Africa. Although the association between ENSO and NDVI has been well-studied, such analyses are usually performed at the regional (e.g. Martiny et al 2009, Brown et al 2010) and/or seasonal time-scales (e.g. Williams and Hanan 2011 – they work with net photosynthesis computed from the Simple Biosphere model and not NDVI –, Kogan 2000), or focus on the impact of particular ENSO events (e.g. the 1997/1998 event in Anyamba et al 2001, 2002, Verdin et al 1999).

In this article we present the NDVI, rainfall and Sea Surface Temperatures (SST) data used. Then we analyse the relationship between NDVI and rainfall at a monthly time-step over the whole of Africa. We also assess the link between the timing of the ENSO teleconnections and the pattern in NDVI response. Finally we discuss the findings in the context of the African continent as a whole.

2/ Methods:

The Normalized Difference Vegetation Index (NDVI) data were obtained from the FEWS NET Africa data portal (http://earlywarning.usgs.gov/fews/africa/index.php). This portal provides 10-day composite NDVI images of Africa at 8 km spatial resolution from July 1981 to present. NDVI data have been collected by the Advanced Very High Resolution Radiometer (AVHRR) sensor onboard the National Oceanic and Atmospheric Administration (NOAA) satellites, and have been processed by the Global Inventory Monitoring and Modeling Studies group (GIMMS, Tucker et al 2005) at the National Aeronautical and Space Administration (NASA). NDVI is calculated from the near-infrared (NIR) and red (VIS) top-of-atmosphere reflectances, using the following algorithm: NDVI = (NIR - VIS)/(NIR + VIS). Values for vegetated land generally range from about 0.1 to 0.7, with values greater than 0.5 indicating dense vegetation. Data have been corrected for (1) stratospheric aerosols due to volcanic eruptions during April 82-Dec 84 and June 91-Dec 93, and (2) artifacts due to satellite drift which is especially important in tropical regions (Pinzon et al 2004). The same desert calibration has been applied for all the sensors (NOAA7 to NOAA17). No correction has been applied for atmospheric effects due to tropospheric aerosols, water vapor, Rayleigh scattering or stratospheric ozone. Maximum value compositing has been used, with a forward binning procedure implemented.

For our purposes we selected the period July 1981 – June 2008 and upscaled the data to 16 km resolution and a monthly time-step by simple spatial and temporal averages. Pixels with NDVI mean values < 0.12, corresponding to bare soils and desert areas, were excluded from the study. These areas are the Sahara, the Namibian coast, Northern Kenya, Northern Somalia and north-eastern Ethiopia.

Figures 1a and 1b presents the months of mean green-up and dormancy onsets of vegetation at the 16 km scale. Following Philippon et al (2007), the green-up (dormancy) onset is defined as the month when NDVI reaches up (down) to the annual mean level. More complex methods based on logistic (Zhang et al 2003), or quadratic (Brown and de Beurs, 2008) functions, or on thresholds (Vrieling et al 2011) have been applied in other studies to more accurately detect these two phenological transition points. At the monthly time-step, however, our simple method leads to results which are consistent with those obtained in the above-mentioned studies. Where bimodal regimes exist, only the green-up and dormancy onsets that respectively follow and precede the lowest mean monthly NDVI value have been retained. This artificially increases the vegetative season duration but there are years and regions for which the short dry season is sometimes suppressed (in 1997/1998 in East Africa for example, Anyamba et al 2002).

Green-up (Figure 1a) starts in March north of the equator and shifts northward to the Sahara margins in August, at an average rate of ~0.05 day per kilometer according to Zhang et al (2005). South of the equator (Madagascar included), green-up is much more uniform with huge areas showing an onset in November or December without any clear north-south propagation The Congo basin, Kenya, South Uganda, and North Tanzania equatorial regions subject to bimodal regimes experience a main green-up onset by October-November. Lastly, the two winter rainfall regions located at the northwest and southwest regions of Africa, experience a green-up start in December and June respectively. Note that in South Africa, the transition between winter and summer regimes is abrupt and influenced by the presence of the Cape Fold Mountains (~2000 m). These results are consistent with those obtained by Zhang et al (2004) and Zhang et al (2005) using MODIS NDVI. The dormancy onset (Figure1b) is much more homogeneous than the pattern found for the onset of green-up. Dormancy onset occurs in October-November in tropical Africa north of the equator and in the winter rainfall region of South Africa. It occurs in May-June south of the equator, in East Africa as well as in the winter rainfall region of Northern Africa. In the rest of the study area, those pixels/months which did not fall within the vegetative season (i.e. between the green-up and dormancy months) were excluded from the analysis. This ensured that we interpreted signals in NDVI that were truly related to vegetation photosynthetic activity and not to soil reflectance values, for example.

Rainfall data used in this study originate from the Global Precipitation Climatology Center (GPCC, http://gpcc.dwd.de/) which provides several gauge-based gridded monthly precipitation data sets for the global land surface, in different spatial resolutions. We selected the GPCC full data reanalysis product (Rudolf and Schneider 2005) which compiles the most comprehensive global collection of in situ monthly precipitation data from 1901 to 2009. We chose the 0.5° x 0. 5° spatial resolution and extracted grid-points covering Africa and Madagascar, for the period January 1981-December 2008. Figure 2ab presents the mean annual rainfall field and the number of stations documenting each grid point. Over that period and area, the number of stations has gradually decreased from ~4200 in January 1981 to ~1150 in December 2008; a decrease attributed to the delay in the delivery and processing of data at GPCC. This variation in station density may generate temporal and spatial inhomogeneities and affect the interannual variability analyses. However, given that the impact on Africa of the ENSO is studied first through NDVI and that the more homogeneous 50-year precipitation dataset elaborated by GPCC in the framework of the VASClimO (Variability Analysis of Surface Climate Observations) research project (Beck et al 2005) has very few stations in Africa, the full data reanalysis product has been preferred over that of VASClimO .

Finally, the Niño3.4 (N3.4) sea-surface temperature (SST) index was downloaded from the Climate

Prediction Center database (http://www.cpc.ncep.noaa.gov/data/indices/). It documents the sea-surface temperature over the area 5°N-5°S/170-120°W and has been computed from the ERSST V3b SST database (Smith et al 2008). We selected the period January 1981 – December 2008 and a monthly time-step. We upgraded data to a monthly overlapping, 3-month time-step. According to Larkin and Harisson (2002) the ENSO seasonal cycle can be decomposed into 6 phases: PRE (till ~December -1), ANTE (~December-1 to March0), ONSET (~March0 to July0), PEAK (~July0 to December0), DECAY (~January+1 to April+1) and POST (from May+1). Our analyses focuses on the ONSET, PEAK, DECAY and POST phases mainly. We are aware that other ENSO 'representative' indexes such as the Multivariate ENSO Index (MEI) also exist and that recently distinct types of ENSO variability (e.g. Eastern-Pacific and Central-Pacific), having somewhat different timings and impacts, have also been highlighted (Kao and Yu 2009, Newman et al 2011, Ren and Jin 2011). However the objective here is to provide a general picture of the teleconnection with ENSO for Africa as a whole. Hence, our results are not optimized nor refined for the different regions of Africa nor according to the different types of ENSO.

3/ Results:

a/ Vegetation photosynthetic activity sensitivity to rainfall :

The ENSO impact on vegetation is mainly through a modulation of rainfall. To properly interpret the ENSO – vegetation teleconnection, we assess first the sensitivity of vegetation to rainfall. Figure 3ab presents the monthly correlation maps between monthly overlapping, 3-month rainfall amounts and monthly NDVI with one-month lag (e.g. the April-May-June rainfall amount is correlated with July NDVI).

The insignificant correlations have not been masked out deliberately to preserve the spatial patterns we are interested in highlighting, and to show the months and regions where the vegetation is active but unrelated to ENSO. Note however that the correlation value significance threshold at the 95%

confidence level is |0.367|.

Such maps have never been produced before and carry interesting new insights as compared to maps produced in previous studies at the annual time-scale (e.g. Camberlin et al 2007) or regional spatial scale (e.g. Brown et al 2010). We selected a one-month lag because it is the lag for which the correlations between vegetation and rainfall mean seasonal cycles are the highest for most of the pixels whatever the vegetation type (not shown). This is coherent with findings by Martiny et al (2006) and Klein and Röhrig (2006) who show for several semi-humid and semi-arid regions in Western, Eastern and Southern Africa that the vegetation response usually lags behind rainfall by one to one-and-a-half months. Similarly, we selected 3-month cumulative rainfall because this measure has already been found to be correlated best with NDVI in semi-arid environments in particular (Nicholson et al 1990, Klein and Röhrig 2006). Indeed, vegetation does not respond directly to rainfall but to soil moisture which is integrative of rainfall accumulated over several months (Malo and Nicholson, 1990).

Vegetation sensitivity to rainfall is the highest for the tropical semi-arid environments, i.e. the Sahelian band from June to November (Figure 3a), Eastern Africa, Southern Africa south of 18°S and Madagascar from November to June (Figure 3ab). Correlations are above 0.5 and up to 0.8 in Eastern and Southern Africa. This is consistent with previous findings performed at the annual time-step (Malo and Nicholson, 1990, Martiny et al 2006, Camberlin et al 2007) and suggests that the relationship between annual NDVI and rainfall is strong and linear for areas with an annual rainfall between 200 and 1000 mm. Figure 2a displays the mean annual rainfall amount over the study period while Figure 4 presents the vegetation cover in Africa issued from the GLC2000 project (Global Land Cover, Mayaux et al 2004). It is clear from Figures 2, 3ab and 4, that the match between areas where correlations are above 0.5, the mean annual rainfall amount is between 200-1000 mm and the dominant vegetation cover is open grasslands and crops (rainfed), is good indeed. But the monthly time-step used here points to several interesting points. First, in East Africa which experiences two rainy seasons, one centered on OND (the 'Short Rains') and the second centered on MAM (the 'Long Rains'), the sensitivity of vegetation to rainfall is higher for OND than MAM. This is consistent with Martiny et al (2006) who computed the Rain Use Efficiency for the two seasons and noticed a higher RUE during the Short Rains than during the Long Rains. Second, the sensitivity does not decline in the dry period stretching between the Short Rains and the Long Rains. On the contrary, in Kenya, the highest correlation ($r>0.8$) is observed between NDJ rains and February NDVI (Figure 3b). This can be related to the vegetation time-response to rainfall which is about one month (Davenport and Nicholson 1993, Martiny et al 2006), but also to the shortness of the January-February dry season which can also be relatively wet, as was the case in 1998, and thus sustain high vegetation photosynthetic activity between the two rainy seasons (Linthicum et al 1999, Anyamba et al 2001). Moreover, the JF dry season follows the OND rainy season which shows a very large rainfall interannual variability. That later impacts strongly on vegetation and large NDVI anomalies usually develop and persist for several months due to memory effects. The gradual increase in the sensitivity of vegetation to rainfall (i.e. higher correlations which are also more coherent in space) during the vegetative season is also observed for the Sahel and Southern Africa, and is also an effect of the lagged response of the vegetation to rainfall and of intra-seasonal memory (Philippon et al 2007).

Vegetation sensitivity to rainfall is moderate to high ($\sim 0.4<r<0.7$) in the winter rainfall semi-arid (200-600mm, Figure 2a) environments of the northwestern (Atlantic and Mediterranean coasts of Morocco, Algeria and Tunisia from January to May, Figure 3b) and the southwestern (Atlantic coast of South Africa from June to October, Figure 3a) parts of Africa. For the former region, it is obvious that the highest correlations are observed for areas where cereal crops dominate (wheat mainly, Figure 4). For the latter region, it is interesting to note that at the annual time-scale Camberlin et al (2007) there was no significant correlation between annual NDVI and annual rainfall (see their figure 2). This region includes two different biomes: the Succulent Karoo and the Fynbos biome which are recognized as global biodiversity hotspots (Meyers et al 2000) and respond to rainfall in different ways. Vegetation of the Succulent Karoo biome appears to be the most sensitive (Fox et al 2005). Its growth starts with the first significant rains at the end of the summer, continues throughout the winter, and then drops sharply in spring as rainfall declines (Esler and Rundel 1999). NDVI for that biome usually exhibits high coefficients of variation (Hoare and Frost 2009). Conversely, vegetation within the Fynbos biome exhibits a bimodal pattern with NDVI peaks in August and November (Hoare and Frost 2009) that do not match well with the seasonal cycle of rainfall which varies from a winter regime in the west to a non-seasonal and equinoctial regime in the eastern parts of the Fynbos biome (Rouault and Richard 2003, see areas 2 and 3 in their figure 2). Moreover the relatively long summer drought period appears not to be a limiting factor to photosynthetic activity within the Fynbos biome (Stock et al 1992). These points explain the weak NDVI-rainfall correlation obtained by Camberlin et al (2007) at the annual time-scale and the somewhat lower sensitivity to rainfall of these winter rainfall, semi-arid environments as compared to those in the summer rainfall areas.

Lastly, sensitivity is generally low ($r<0.2$) in sub-humid and humid environments. However, once again, when compared to results obtained at the annual time-step by Camberlin et al (2007), the monthly time-step contributes interesting insights. For instance, a moderate sensitivity in the NDVI signal ($0.3<r<0.6$) is observed at the beginning of the vegetative season in the sub-humid environments (800-1200mm/year, Figure 2a) of Western (~0-10°N) and Southern Africa (~10-18°S) and Madagascar. In Western Africa, the positive correlation pattern moves northward from April to June (Figure 3b) in agreement with the start of the West African Monsoon and the ITCZ migration to the north. In Southern Africa, sensitivity is obvious in November-December (Figure 3a) over Mozambique, East of South Africa and in Zimbabwe, South Angola and Zambia. This pattern is evident as well at the end of the growing season (May-June, Figure 3b). According to the land cover map in Figure 4, these regions, at the transition between humid and semi-arid environments, are a mosaic of croplands, woodlands and shrublands and are not covered by evergreen forest, for which the NDVI is known to saturate and to be less sensitive to rainfall variation. This is exemplified by Central Equatorial Africa (~12°S-5°N/8-30°E) where the annual rainfall amounts are above 1200mm/year (Figure 2a), and the vegetation cover is dominated by evergreen lowland forest (Figure 4). Most of the pixels have NDVI-rainfall correlations (Figure 3ab) close to zero or even negative, suggesting that above normal rainfall amounts are conducive to below normal photosynthetic activity. This point is discussed in section 4.

b/ Impact of ENSO in Africa: insights from the vegetation photosynthetic activity

Following the preceding NDVI-rainfall analyses, the impact of ENSO in Africa is assessed by computing correlations between monthly overlapping, 3-month SST values over the Niño3.4 region (N3.4 hereafter) and monthly NDVI values. Results are presented in Figure 5ab. The significance of the correlations is not presented at that stage because masking those pixels that have insignificant correlation values but which are of a consistent sign would mask or reduce the spatial patterns we are interested in showing. Nonetheless as for Figures x the correlation value significance threshold at 95% is indicated in the color bar.

To give confidence to and interpret the teleconnections highlighted between NDVI and N3.4, analyses have been carried on rainfall too. The 0-month lag correlations, between the overlapping, 3-month N3.4 values and the coarse and interpolated GPCC 3-month rainfall amounts (i.e. AMJ N3.4 vs AMJ rainfall), have been computed, and then compared to the correlations between NDVI and N3.4 (i.e. AMJ N3.4 vs July NDVI). Then, monthly synthetic maps (Figure 6ab) have been constructed according to the sign and significance (at the 95% level) of the correlations between NDVI and N3.4, and rainfall and N3.4, applying the following procedure: for each monthly map, pixels for which the correlation between NDVI and N3.4 is positive (negative) and significant are ascribed the value of 2 (-2). Similarly, pixels for which the correlation between rainfall and N3.4 is positive (negative) and significant are ascribed the value of 2 (-2). Pixels with insignificant correlations are ascribed a value of -1 or 1 according to the correlation sign. The addition of the NDVI and rainfall coded maps leads to monthly synthetic maps where values vary between -4 and +4. Areas with values >=|3| are of particular interest since NDVI and rainfall correlations with N3.4 are of the same sign and are significant in one field at least. Note that given the difference of spatial resolution between NDVI (~16 km) and rainfall (~50km) data, several pixels of NDVI belong to the same pixel of rainfall. This can somewhat enhance the signal in the synthetic maps. Note as well that, for example, the 'July' synthetic map displays the AMJ N3.4 correlation with July NDVI and AMJ rainfall, and therefore accounts for the mean one-month lagged vegetation response to rainfall. Figure 5ab, suggest that Africa can be divided into three main regions according to the sign and timing of the correlations between NDVI and N3.4. These are the summer rainfall regions, the winter rainfall regions and the equinoctial rainfall regions.

<u>i) ENSO impact on vegetation photosynthetic activity in summer rainfall regions :</u>

The two summer rainfall regions of Africa are located between 35°S-10°S ('Southern Africa') and 8°N-17°N/20°W-40°E ('Sudan-Sahel'). The former experiences a vegetative growing season from ~December to May while the latter experiences a vegetative growing season from ~June to November (see Figure 1ab, and Figure 7 where the NDVI seasonal cycles are provided for 7 different regions across Africa). Generally speaking, the vegetation photosynthetic activity of the two regions tends to be dampened (increased) during ENSO (LNSO) years as indicated by the negative correlations with N3.4 (Figure 5ab and 7).

In Southern Africa, negative correlations with N3.4 appear as early as December (January) at the border between South Africa, Zimbabwe and Mozambique (the leeward region of Madagascar). By March, these correlations have intensified and spread over the whole region south of 18°S (Namibia/Angola border area), while north of 18°S (and to the windward side of Madagascar), positive correlations are recorded. It is noteworthy that according to the vegetation map of GLC2000 (Figure 4), the transition from shrub/grass dominant vegetation (in the south) to tree dominant vegetation (in the north) is located near 18°S. From April to June the negative correlations gradually shift to the north and the east reaching Angola, Zambia and Malawi, then the north of Mozambique and the south of Tanzania.

As indicated by the synthetic maps (Figure 6b), the correlation patterns between N3.4 and NDVI on the one hand, and between N3.4 and rainfall on the other hand, are similar (dark shades of red or blue, values <-2 or >2). It is noteworthy that the agreement is not limited to the semi-arid regions south of 18°S but also to the sub-humid and humid areas to the north where the vegetation sensitivity to rainfall has been shown to be moderate at the beginning and end of the vegetative season (Figures 1b). The north-south dipole in January-February-March is obvious and as a consequence can't be attributed to vegetation memory effects only. These results agree with and complement the results from several previous studies that have explored the impact of ENSO on vegetation and rainfall in Southern Africa. For example, the north/south dipole in the NDVI/ENSO correlation pattern is evident in the studies by Anyamba and Eastman (1996) and Anyamba et al (2001), who have mapped the evolution of NDVI anomalies during the ENSO/LNSO years 1986/1989 and 1997/1998. It is also coherent with correlation maps of Williams and Hanan (2011) for the season DJF where the limit around ~18°S is clearer during LNSO than ENSO events. Similarly, Brown et al (2010) obtain coherent patterns of negative correlations between the Multivariate ENSO Index (MEI) and NDVI cumulated over March-May at the border between South Africa, Zimbabwe, Mozambique, and in North (South) Namibia (Angola). These authors obtain either a non-significant or positive correlation between March-May NDVI and MEI in South Africa and Madagascar. However, it is obvious from our results that ENSO has its strongest negative impact over these two regions from January to March and not March to May. For that latter period correlations are close to zero and the vegetative season has come to an end in part of South

Africa (see the May map). This once again points to the importance of considering a monthly time-step to accurately follow the spatial evolution of the ENSO impacts.

The mechanisms sustaining the ENSO/rainfall teleconnection in Southern Africa have been documented in numerous studies. At the seasonal time-scale, and when analysing both observations and AGCM (Atmospheric General Circulation Model) outputs, Richard et al (2000) and Mason (2001) note that in the recent context of warmer SST over the southern oceans, (i) a bipolar pattern between Southern Africa and the South West Indian Ocean develops during ENSO years with decreased (increased) convection and rainfall over the continent (ocean), and (ii) the subtropical high-pressure belt is also weakened, leading to reduced moisture fluxes toward the continent. Working at the intra-seasonal time-scale, Fauchereau et al (2009) and Pohl et al (2009) show that the ENSO/rainfall teleconnection at the seasonal scale arises from a modulation of the tropical-temperate interactions and in particular of the frequency of the Tropical-Temperate Troughs (TTT) which are the dominant rain-bearing systems.

Concerning Madagascar, it must be noted that at the monthly time-step, the teleconnection with ENSO shifts from negative at the beginning of the vegetative season (January) to positive at the end (May, Figures 5-6b). A similar switch from positive correlations in November to negative ones in December is observed in South Africa. This agrees with Richard et al (2002) who showed that rainfall anomalies during the pre-season (October) tend to be out-of-phase with rainfall anomalies during the rainy season (December-April), which is a pattern and mode of variability significantly related to ENSO.

As compared to Southern Africa, the impact of ENSO on vegetation photosynthesis in Sudan-Sahel (Figure 5a and 7) is weaker and less spatially coherent. This is consistent with Propastin et al (2010) and Williams and Hanan (2011) who found the West African vegetation to be less vulnerable to ENSO warm events than the Southern Africa vegetation, or with Philippon et al (2007) who observe a weak negative correlation between the 1st mode of NDVI variability over West Africa (depicting the July to October NDVI variability over the Sahelian domain) and ENSO. This is partly explained by the phasing of the rainy and vegetative seasons with ENSO which is either in the ONSET or POST phases for West Africa and not in the PEAK or DECAY phases as is the case for South Africa. Another possible explanation of the weak correlations could be the decadal variations of the climate background state, which were shown to affect the teleconnection between ENSO and Sahelian rainfall (Janicot et al 2001, Rodriguez-Fonseca et al 2011). However, it can't be the main explaining factor since the effect of decadal-scale climatic oscillations is also found in Southern Africa rainfall (Richard et al 2000), although the correlations between NDVI and ENSO remain consistent in this region). In July-September, the most consistent signals are observed at the two extremities of the Sahelian band, i.e. Senegal and Mali, and the border between Sudan, Uganda and Ethiopia. There isn't a clear continuity of the ENSO impact over the whole Sahelian band, a feature also apparent in the composite maps by Williams and Hannan (2011) for the June-August season. This could be explained by the fact that according to Brown et al (2010) the ENSO/LNSO events impact more strongly the start of the vegetative season (delayed during warm events) than its core, particularly over Senegal and Mali (see their figure 7). But it could also be due to a weak response in rainfall to N3.4 during the core of the rainy season. Indeed, looking at the synthetic maps (Figure 6a), it is obvious that in Central Sahel few values are above |2| which suggests that the N3.4-rainfall correlations themselves are barely significant. This is again consistent with findings by Camberlin et al (2001) who observed a similar discontinuity in the ENSO impact with grid-points in Niger and Sudan which show insignificant correlations with ENSO (see their figure 4) in JAS. The stronger impact of ENSO on NDVI in East Sahel than in West and Central Sahel (which is apparent in the synthetic maps as well Figure 6ab, dark shades of red) is a fact pointed out as well in the precipitation patterns by Ward (1998) and Camberlin et al (2001). These patterns are related to a teleconnection of the East Sahel/Ethiopian rainfall with the Indian summer monsoon. However, even in Ethiopia where the correlations are best, patterns are not uniform and coherent across the country. This is consistent with the study by Gissila et al (2004) who have shown that the correlation between rainfall and SST in the Pacific varies spatially and is strongest for the western parts of the country. Janicot et al (1996, 2001) and Rowell (2001) show that the impact of ENSO on West Africa is as a result of anomalies of zonal divergent circulation between the tropical Pacific, Atlantic and Indian oceans that favor subsidence over the Sahel limiting moisture advection to the region and convection within the ITCZ. Mohino et al (2011) suggest that while ENSO reduces Guinean rainfall during the monsoon pre-onset through anomalies of subsidence over the Gulf of Guinea, it reduces Sahelian rainfall during the monsoon peak and withdrawal through equatorial Rossby waves from the maritime continent. The negative impact of ENSO on summer rainfall in Uganda and North West Kenya has been documented by Ogallo (1988), Camberlin (1995), Philips and McIntyre (2000) and Indeje et al (2000) who stressed that the importance of the JAS rainfall peak to the farmers is equal to the peaks in MAM and OND. This pattern of negative correlation fits very well with the region of intensive cultivation seen in GLC2000 Land Cover Map of Africa (Figure 4). However, in the study by Williams and Hanan (2011), this ENSO impact on net photosynthesis does not appear, probably because of the seasonal time-scale considered (JJA and SON).

In October, two dipoles appear in the N3.4-NDVI correlation map (Figure 5a and 7): a north-south dipole around ~12°N, and a west-east dipole around ~40°E. The first dipole between the Sahelian and Guinean bands, although implying weak correlations, suggests that during ENSO years (as compared to LNSO years), the southward retreat of the rain belt could be more rapid. Then, the teleconnection with ENSO seems stronger at the end than at the beginning of the vegetative/rainy season. This can be attributed to a higher vegetation sensitivity to rainfall as shown in section 3a (Figure 3a) as well as memory effects but also to the fact that ENSO has entered into its PEAK phase. The emergence of the 2^{nd} dipole between West Ethiopia/Uganda and East Ethiopia/Somalia can be attributed to two factors: vegetation memory and the set-up of equinoctial rainfall anomalies.

Indeed, in West Ethiopia and Uganda, the October NDVI negative anomalies in ENSO years are in line with the NDVI and rainfall anomalies that have emerged in July. On the contrary, the East Ethiopia and Somalia NDVI positive anomalies are in line with the rainfall anomalies affecting the Short Rains (onset in October), with a rapid response of the vegetation to rainfall anomalies after the long JJAS dry season. This is discussed further in section c devoted to equinoctial rainfall regions.

ii) winter rainfall regions :

The two winter rainfall regions of Africa are located respectively in South Africa (primarily along the Atlantic coast) and Northwestern Africa (along the Atlantic and Mediterranean coasts) respectively. Vegetative growing seasons span the periods from July to October and January to May respectively (Figure 1). As opposed to the summer rainfall semi-arid regions, correlations with N3.4 are weak and mainly positive (Figure 5ab). Enhanced (diminished) vegetation photosynthetic activity is expected during ENSO (LNSO) years. This could be due to a lower ENSO impact on rainfall but also to the vegetation itself since shrubs dominate most of the winter rainfall areas (as opposed to grasses which dominate vegetative cover in the summer rainfall, semi-arid environments). Shrubs are known to be less sensitive to rainfall variations and also to exhibit a lower amplitude in NDVI values between seasons. For South Africa (Figure 5a), it is interesting to note that the signal appears in the Succulent Karoo region (i.e. between 31°S and the Namibian border) first, then in the more southerly Fynbos region which is impacted mainly in August. This agrees with the higher sensitivity of the more arid Succulent Karoo biome to rainfall as compared to the Fynbos biome (Fox et al 2005). For Northwestern Africa (Figure 5b), the signal is less clear and coherent. While the Mediterranean-facing region of Morocco and Algeria show positive correlations between NDVI and N3.4, the region which faces towards the Atlantic exhibits a negative correlation between these variables.

Little is known about the impact of ENSO on rainfall and vegetation over these two semi-arid regions as most of the studies devoted to African rainfall variability have focused on the summer rainfall regions. Most of the precipitation in the South African winter rainfall region falls from April to September. Although NDVI is not significantly correlated with ENSO before July, the synthetic maps in Figure 6a suggest that rainfall in June is positively and significantly correlated with ENSO. This is consistent with the findings of Philippon et al (2011) who have recently highlighted a positive correlation between ENSO and the MJJ rainfall amount (r~0.5 over the period 1979-1999). The analysis of the characteristics of the wet spells and the associated atmospheric dynamics suggests that during ENSO years the rain-bearing systems (extratropical troughs mainly) in MJJ are more frequent, deeper and are shifted towards the north, thus carrying more rainfall over the region. Northwestern Africa records its rainfall season from October to April with the highest falls in November-February. Looking at the synthetic maps (Figure 6b), the rainfall-N3.4 and NDVI-N3.4 correlation patterns are in good agreement for the Mediterranean-facing region as suggested by the dark shades of blue: the ENSO-NDVI and ENSO-rainfall correlations are positive and significant. This is consistent with the findings of Mariotti et al (2002) who have analysed the composite pattern in seasonal rainfall in northwestern Africa according to ENSO warm and cold events. They have observed that the teleconnection shifts from positive to negative between autumn and spring. Thus, the positive correlation we observe between ENSO and NDVI could be a combination of the vegetation sensitivity to autumn rainfall added to memory effects. The agreement between ENSO-NDVI and ENSO-rainfall correlations is less for the Atlantic-facing region as suggested by the light shades of orange (negative correlations), but the ENSO-NDVI correlations themselves are lower in absolute value than those observed in the Mediterranean-facing region. It is noteworthy as well that the area of negative correlations confined to the Southeast of Morocco in January has spread towards the North in February-March. Lamb and Peppler (1991) have obtained weak positive correlations between the Southern Oscillation and the November-April rainfall in the Moroccan

Atlantic coast over the period 1933-1985. Knippertz et al (2003) have studied the impact of ENSO on springtime Europe and Northwestern Africa rainfall and the decadal changes in the teleconnection. Over the 1962-1987 period, they observe that springtime rainfall (MAM) is negatively correlated with ENSO with the largest correlations observed for the Atlantic-facing region. However, the dipole seen with NDVI between the Atlantic and Mediterranean regions does not appear in any of the three studies mentioned. This could be attributed to the different study periods considered but also to the different types of vegetation occupying the Atlantic and Mediterranean facing regions. According to GLC2000 (Figure 4), croplands dominate in the Moroccan Atlantic facing region where wheat is grown and irrigated if the water resources are sufficient. This can partly disturb the NDVI response to climate variability.

iii) equinoctial rainfall regions :

The equatorial regions of Africa, namely East Africa (10°N-10°S/32-45°E) and Central Africa (~12°S-5°N/8-32°E) have equinoctial rainfall regimes, i.e. two rainy seasons coinciding with the northward and then the southward passage of the Inter Tropical Convergence Zone which produces rain in October-December (the Short Rains) and March-May (the Long Rains) in East Africa, and in February-May and September-November in Central Africa (Nicholson and Grist 2003, Balas et al 2007).

The impact of ENSO on the East African vegetation photosynthetic activity and rainfall has been well-documented. During the Short Rains, warm ENSO events are associated with positive NDVI anomalies. NDVI anomalies usually emerge in October over East Ethiopia / South Somalia first (figure 5a and 7) and can be related to anomalies that have affected rainfall as early as September (figure 6a). NDVI anomalies spread southward to North and East Kenya by November, then to North Tanzania by January (figure 5b). Rainfall-N3.4 and NDVI-N3.4 correlations patterns are in good agreement as indicated by the dark shades of blue in the synthetic maps (figures 6ab).

Moreover, the signal is strongly coherent in space. For instance, even if NDVI is positively but not significantly correlated to N3.4 (e.g. in January along the Kenyan coast), anomalies in rainfall are significant. In February (figure 5b), NDVI anomalies start to fade away over Tanzania first, then in Kenya and South Somalia in March. Thus, these latter regions experience large NDVI anomalies for ~4 months. These results agree with previous studies on NDVI and rainfall performed at the seasonal scale for this region and season. For example, the NDVI anomaly pattern associated with the 1997/1998 ENSO event shown by Linthicum et al (1999) and Anyamba et al (2002) featured strong positive anomalies from December to March in Kenya, and the south parts of Somalia, Ethiopia, Sudan. With regard to rainfall, the teleconnection between equatorial East African (Kenya-Uganda-Tanzania) Short Rains and ENSO has been documented by many authors, including Indeje et al (2000), Mutai and Ward (2000). The teleconnection is positive (ENSO years are associated with above normal rainfall) and operates during the entire rainy season through a modification of the Walker cell circulation over the Indian Ocean. The low-level (high-level) winds blowing to the east (west) along the equator are weakened or turn westward (eastward), bringing moisture to the region and favoring first convection and then rainfall. Hutchinson (1992) studied the rainfall of the 'Der' rainy season (SOND) in South Somalia and observed significant negative correlation between JJA and SON values of the Southern Oscillation Index. Mapande and Reason (2005) focused on Western Tanzania, a region at the transition between the opposite-signed ENSO-impacted Eastern and Southern African regions, and reported that above normal October-April rainfall was associated with warm ENSO events.

The correlation patterns of NDVI-N3.4 during the Long Rains (MAM, Figure 5b) are radically different from those that occur during the Short Rains. The strength of the correlation is also lower and less coherent in space and time. Warm events are loosely associated with negative NDVI anomalies in April from Northern Tanzania to South Somalia. From March to April correlations switch very quickly from positive to negative (see Figure 7 as well). By May, the negative correlations have weakened and in June, sparse positive correlations appear in Northwestern Kenya, Somalia and East Ethiopia. The synthetic maps (Figure 6b) suggest that ENSO warm events are indeed associated with negative rainfall anomalies in March over the whole region (South Somalia-Kenya-North Tanzania) and in April over Tanzania mainly, while positive rainfall anomalies occur in May to the North. Camberlin and Philippon (2002) studied the coherency and predictability of the Long Rains. While they showed a fair degree of spatial coherency, their temporal coherency was low. Because of this they called for separate teleconnection analyses for March-April and May. Moreover, they observed a negative correlation between Niño 3 and the March-April rainfall amount and a positive correlation for May rainfall which is consistent with our NDVI-N3.4 correlation maps and our synthetic maps.

Over Central Africa, the ENSO signal is far less prominent. North of the equator (~ 0°-5°N), the vegetative season spans from ~ April to November (Figure 5ab) in response to the March-May and August-October rainy seasons (the main dry season is in DJF and the minor one in JJ). Generally speaking, the correlation patterns for that region and these months (April-November) are noisy. The only coherent signals are observed in (i) March-May as a band of negative correlations that propagates from the equator to 7°N and is replaced by a band of positive correlations in May, and (ii) August-September as negative correlations to the east of the Democratic Republic of Congo (DRC). Comparing first these patterns to the ones in Figure 3ab, it must be noticed that the NDVI over the region showing negative correlations with ENSO in March-May is actually sensitive to rainfall variations, but not the NDVI over the eastern DRC in August-September. Evidence in the synthetic maps, shown in Figure 6ab, suggests that there is good agreement as well between the NDVI-N3.4 and rainfall-N3.4 correlation patterns in March-May as depicted by the light orange and red shadings. The agreement is weaker in May for the region with positive NDVI-N3.4 correlations (Figure 5a) as well as in August to the east of the DRC as depicted by the white pixels. The good match between the NDVI-rainfall, NDVI-N3.4 and rainfall-N3.4 correlation patterns in

MAM suggests that ENSO might modulate the northward propagation of the ITCZ during the boreal spring with propagation slowed down during warm events. South of the equator (~ 12°S-0°), the vegetative season spans from ~ October to May (Figure 1ab and Figure 7) in response to the September-November and February-May rainy seasons (the main dry season is in JJA and the minor one in JF). Spatially coherent correlations between NDVI and N3.4 are mainly observed in February (Figure 5b): warm events in the equatorial Pacific appear to be associated with an enhanced vegetation photosynthetic activity over all of Central Africa during that month. This is in line with the results obtained by Los et al (2001) who have mapped, at global scale, the progression of NDVI, precipitation and temperature anomalies during the first 17 months of the 2.6-yr ENSO cycle. At t=9 months, positive anomalies of NDVI are obvious over the whole of the Congo basin (see their figure 2). Over the preceding and following months, i.e. January and March, the correlation pattern features dipoles: a west/east one with negative/positive correlations on both sides of ~ 20°E and a north/south one with negative/positive correlations on both sides of ~ 4°S respectively. However, from Figure 3b it appears that vegetation photosynthetic activity during these three months is barely sensitive to rainfall variations (low or even negative correlations as depicted by the white and yellow shadings) except in Angola (note that it is mainly covered by deciduous woodlands and not by rainforests, Figure 4), and the north of Congo and DRC in March where positive NDVI-rainfall correlations are obvious. Moreover, the spatial coherence seen in the February NDVI-N3.4 correlation maps is less obvious in the synthetic maps (Figure 6b). For instance, in the central region of the DRC the positive correlation observed between NDVI and N3.4 is not observed between rainfall and N3.4 (or is of the reverse sign, i.e. negative) as indicated by the white pixels. Similarly, in the study by Los et al (2001) the ENSO-rainfall correlations are less marked and coherent than the ENSO-NDVI ones. The dipoles seen in January and March seem more robust: in particular in March, the shadings of red over the Gabon and the north Congo, and of navy blue over the western parts of Angola and DRC indicate that NDVI-N3.4 and rainfall-N3.4

correlations are of the same sign and significance. While warm events in December-January in the equatorial Pacific are associated with high rainfall amounts which produce high NDVI in March over the western parts of Angola and DRC, they are associated with low rainfall amounts and subsequently low NDVI over Gabon / north Congo.

As compared to the other African regions, the climate of Central Africa and its variability has been the subject of very few studies. This is partly due to the relative paucity of long-term climate data in the region. Malhi and Wright (2004) have studied the trends in precipitation and temperature of the tropical rainforest regions (namely South America, South-East Asia and Central Africa) over the last 40 years as well as the relationships with ENSO. Whereas ENSO appears as the primary driver of temperature variations in all the tropical rainforest regions, and of precipitation in South America and South-East Asia, they couldn't find any significant relationship between ENSO and precipitation in Central Africa. However, it should be noted that Malhi and Wright (2004)computed interannual correlations for all months which doesn't take into account potential seasonality in the ENSO-rainfall relationships. The Central Africa rainfall - ENSO relationships have also been documented in studies by Nicholson and Kim (1997), Poccard et al (2000), Camberlin et al (2001), and more specifically in the studies by Balas et al (2007) and Misra (2010). Most of these studies except Misra (2010), focus on the western parts of Central Africa where the raingauge network is denser (Figure 2b). Camberlin et al (2001) and Balas et al (2007) use raingauge data only and show that negative rainfall anomalies in OND and/or DJF over Gabon and Congo are associated with warm events in the equatorial Pacific. Using rainfall data from raingauges, satellite measurements (Tropical Rain Measuring Mission 3B42), and simulations using the Center for Ocean-Land-Atmosphere studies coupled climate model, Misra (2010) shows that positive anomalies of rainfall in DJF are recorded over the eastern parts of the DRC during warm events. These rainfall anomalies result from the development of anomalous upper level divergent winds over the western Indian Ocean. Hence, our findings agree well with these results.

4/ Discussion and summary

The aim of this study was to provide a precise and updated picture of the timing and patterns of ENSO impacts in the whole of Africa during the last three decades. We used the Normalized Difference Vegetation Index rather than rainfall for that purpose. This was because NDVI has a high spatial resolution, documents the whole of Africa, and is more frequently updated than rainfall databases. It also has the advantage of being an integrator of rainfall accumulated over several weeks. Therefore, using NDVI brings out signals that are potentially stronger, and occur at a higher spatial resolution, than when using available rainfall products. However, one of the drawbacks of using NDVI is that signals are often difficult to explain for the humid areas where vegetation does not respond that readily to rainfall variations (e.g. Central Africa) and for the cultivated areas under irrigation where water supply may induce variations in photosynthetic activity likely to obscure the natural response to climate.

In a first step we have used correlation analyses so assess the sensitivity of NDVI to rainfall variability at the monthly time-step considering a one-month lag between rainfall accumulated over three months and monthly NDVI. Although this lag is not strictly valid for every region of Africa, our results in many ways confirm those obtained previously. For example, at the monthly time-step, the NDVI-rainfall relationship is the strongest (r = 0.5 to 0.8) for environments receiving between 200 and 1000 mm per year, such as the semi-arid environments of the summer (or equinoctial) rainfall regions of the Sahel, the Horn of Africa and Southern Africa. But most importantly, several new features have been highlighted. First, for those semi-arid environments, correlations increase during the vegetative season. In East Africa which experiences two rainy seasons, the vegetation sensitivity is higher during the Short Rains (OND) than during the Long Rains (MAM). This could be explained by a higher variability of the Short Rains as compared to the Long Rains, but also by the previous June-September long dry season which erases part of the inter-season memory effects that could occur between the Long Rains and the Short Rains. Actually for that region, the sensitivity of vegetation to rainfall variability is the highest in January – February, the short dry season. Although this signal is partly related to memory effects in response to the high interannual variability of the Short Rains, the short dry season shows a high variability as well and can be very wet as in 1998. Second, the vegetation of the more humid environments (1000 – 1200 mm per year) appears sensitive to rainfall variability at the beginning of the vegetative season with correlation values around 0.3-0.6. This point has never been shown before because previous studies have considered the annual or seasonal time-scales that dampen the signal which is clearly restricted to the first two months of the vegetative season. However, it should be noted that vegetation cover in these environments is not comprised of evergreen forest but of deciduous forest, whose leafing at the end of the dry season may be delayed in years of late onset of the rainy season. Third, the semi-arid environments of the winter rainfall regions located to the northwest and southwest parts of Africa are sensitive to rainfall variability as well, with correlation values around 0.4-0.7. This result suggests that more attention should be given to these regions since they are densely inhabited, sustain an intense agricultural export industry, and because of their location at the transition between the mid-latitudes and the tropics, which is an area that is expected to be strongly affected by climate change (Mc Kellar et al 2007, Giorgi and Lionello 2008). In the very wet environments (>1200mm/year) of Central Africa, the NDVI-rainfall correlations are close to zero or even negative as in October, and January-February over parts of the DRC, suggesting that above normal rainfall are conducive to lower photosynthesis. Although we can't give as much confidence to our results for that region given the scarcity of rainfall data (Figure 2b) and the NDVI data quality (still affected by cloud and water vapour contamination), Graham et al (2003), Huete et al (2006) and Pau et al (2010) studying the response of tropical forest to climate variability in the Republic of Panama, Amazon basin and the Hawaïan Islands respectively, point to the importance of light rather than rainfall or temperature as a limiting factor for vegetation photosynthesis. Actually, the partial correlations computed between NDVI and the total cloud cover amount (from the International Satellite Cloud Climatology Project – ISCCP – database) after having removed the effect of rainfall (not shown) are usually negative for the pixels showing negative NDVI-rainfall correlations. This might explain the negative correlations observed between rainfall and NDVI: indeed, high rainfall amounts are associated with a high cloud cover hence less light. However, the apparent lack of NDVI sensitivity to rainfall in our study could also arise from two other factors: (i) the time response of vegetation that can be greater than the one opted for that study (i.e. one-month) and (ii) the great disparities that exist among the different species in terms of sensitivity and time response to climate variability, and that can weaken the signal. For instance Couralet et al (2010) notice from a survey of semi-deciduous overstory trees in the Mayombe forest of the DRC that while the growth of some species is mainly dependent on the early rainy season rains, the growth of other species is impacted by rains at the end of the rainy season. Moreover, the variability of the length and intensity of the dry season which has not been explored in this study might also play a much more dominant role in the photosynthetic activity of vegetation than that of rainfall accumulated during the rainy season.

In a second step, we have mapped the month by month evolution of the one-month lag correlations between El Niño3.4 index (3-month values) and NDVI (monthly values) over the whole of Africa. The use of a monthly time-step adds important new insights about the timing and patterns of ENSO impacts to the findings of previous studieswhich are based largely on annual or seasonal time-scales and on a regional spatial-scale. Starting from July (the beginning of the peak phase of ENSO (July 0 - December 0)), to June (the post phase of ENSO (+ May 1)), the teleconnection patterns over the whole of Africa evolve as follows. From July to September, negative correlations between NDVI and N3.4 are observed north of the equator (including the Sahel, Guinean coast, and regions from the northern Democratic Republic of Congo to Ethiopia) but they are not uniform in space and are moderate (~0.3) except towards the east. Conversely, positive correlations are recorded over the winter rainfall region of South Africa. In the period from October-November, negative correlations over Ethiopia/Sudan/Uganda strengthen while positive correlations emerge in the Horn of Africa, over the Sudanian/Guinean domains in West Africa, central Africa and the southeast coast of South Africa. Hence, two dipoles appear to be present during warm and cold events. The first is a north/south dipole in West Africa and a latitudinal modulation of convection which moves southwards during ENSO events. The second is a west/east dipole in East Africa and a longitudinal modulation of convection which moves eastwards during ENSO events. By December, end of the peak phase of ENSO, with the settlement of the ITCZ south of the equator, positive correlations over the Horn of Africa spread southward and westward while negative correlations appear over Mozambique, Zimbabwe and South Africa. This pattern strengthens and a dipole at 18°S is well established in January-March (the decay phase of ENSO), with reduced photosynthetic activity during ENSO years south of 18°S and enhanced activity north of 18°S. In the meantime, by ~2°N negative correlations spread northward, while at the northwestern tip of Africa, a west/east dipole is observed as well with positive correlations over Algeria and eastern Morocco and negative correlations over western Morocco. Lastly, at the end of the ENSO decay phase and the beginning of its post phase (April 1 to June 1) a northward (to 10°S) and eastward (to the south of Tanzania) spread of the negative correlations south of 18°S occurs while the positive correlations over equatorial East Africa switch to being negative. Thus, the NDVI/N3.4 teleconnections feature regional-scale dipoles but also propagative patterns both in space (from one region to another one) and time (from one month to another). These patterns have not been identified with such accuracy in previous studies. These patterns in NDVI agree with those for rainfall which have been computed using the GPCC database and gives further support for our results. They suggest that ENSO plays on the location of the ITCZ (its southward and northward but also eastward and westward displacements) and the convection within it during most of the seasonal cycle.

Our confidence in our findings however, is low for Central Africa and northwestern Africa where discrepancies exist between responses to ENSO in NDVI and rainfall. For these two regions, the lack of studies related to vegetation and climate variability are a handicap to the interpretation and evaluation of the robustness of our results. Thus, part of the ENSO signal which we have detected is questionable. Discrepancies between NDVI and rainfall responses to ENSO in parts of Central Africa might be related to 3 factors : (i) the low sensitivity of vegetation to rainfall already discussed earlier in that section, (ii) the quality of the rainfall data and (iii) of the vegetation data. As regards the 2nd point, in-situ rainfall data available in the region are very scarce and irregularly distributed as illustrated by Figure 2b. Hence, rainfall information for most of the grid points is determined by the interpolation of data from a neighbouring grid-point rather than from the average values derived from rain gauges. Some signals, therefore, might be an artificial extension of signals from regions benefitting from a denser network of rain gauges such as the East African Great Lakes, the Cameroon/Gabon or Namibia. One way to circumvent that problem would be to use rainfall estimates derived from satellites. Unfortunately, these estimates, especially those based on infra-red data, are still unreliable for the region. For example, the multi-satellite rain product from the Global Precipitation Climatology Project (GPCP) overestimates by a factor of two the estimates derived from rain gauges from the Global Precipitation Climatology Center (GPCC) (Mc Collum et al 2000). The NOAA-AVHRR NDVI data themselves over the region are compounded by the persistence of clouds which, despite the 10-day 'filtering', contaminate the data and make the vegetation signal uncertain. It would also be worth checking some of these results using other NDVI databases such as the MODerate resolution Imaging Spectroradiometer (MODIS) as well as another vegetation index such as the Enhanced Vegetation Index (EVI). For instance, Huete et al (2002) have evaluated the performance of the MODIS NDVI and EVI products over a wide range of biomes (from the semi-arid grassland of Arizona to the tropical broadleaf forest of Brazil) and compared it to the products derived from NOAA-AVHRR. They note that when compared to NOAA-AVHRR NDVI, MODIS NDVI has a greater seasonal dynamic range over the wet environments and during the wet growing season. They attribute the differences to the atmosphere water vapour content that strongly affects the AVHRR near infrared band and decreases NDVI values. The authors note as well that when compared to MODIS NDVI, MODIS EVI does not become as easily saturated when viewing rainforests. From the climate side, it must be stressed as well that unfortunately (i) the spatial coherence of rainfall in Central Africa is lower than in most other parts of Africa and (ii) its climate variability is generally independent of ENSO (except over its margins and/or in case of powerful ENSO events). For example, the correlation patterns between N3.4 and the ISCCP cloud cover amount (not shown) over Central Africa do not show any significant and positive values in JFM as evident in NDVI. Still, there are interesting (and probably real) vegetation signals over the region: first, to the south towards Angola in February-March, with positive NDVI-N3.4, rainfall-N3.4 and NDVI-rainfall correlations observed; second, along the west coast and to the north with negative NDVI-N3.4 and rainfall-N3.4 and cloud cover – N3.4 (not shown) correlations evident from January to March from Gabon/Congo to the northern DRC, Cameroon and Central Africa Republic suggesting a modulation of the ITCZ northward propagation by ENSO events; and third, possibly towards the eastern DRC. All these regions/seasons have seldom been documented previously and deserve more attention in future studies. So far, our study has identified interesting teleconnection patterns and pointed out the main regions / months at risk during ENSO/LNSO events. However, beyond the general picture that emerges of the ENSO impact on Africa, patterns are not necessarily the same from one event to the other (Myneni et al 1996, Kogan 2000). Indeed, we have not explored the possible asymmetries in patterns between ENSO and LNSO events or between the different ENSO events (e.g. the 1997/1998 ENSO event didn't have had the expected repercussion on rainfall in Southern Africa, Lyon and Mason 2007) or types of ENSO (i.e. Central and Western, Ren and Jin 2011) since we have worked under an assumption of linearity.

References

Ali, A., Amani, A., Diedhiou, A., & Lebel, T. (2005). Rainfall estimation in the Sahel. Part 2: Evaluation of Raingauge Networks in the CILSS Countries and Objective Intercomparison of Rainfall Products. J. of Applied Meteor., **44**, 1707-1722.

Anyamba, A., & Eastman, J.R. (1996). Interannual variability of NDVI over Africa and its relation to El Niño/Southern Oscillation. International Journal of Remote Sensing, **17**, 2533-2548.

Anyamba, A., Tucker, C.J., & Eastman, J.R. (2001). NDVI anomaly patterns over Africa during the 1997/ 98 ENSO warm event. Int. J. Remote Sensing, **22**, 1847-1859.

Anyamba, A., Tucker, C.J., & Mahonney, R. (2002). From El Niño to La Niña: Vegetation Response Patterns over East and Southern Africa during the 1997–2000 Period. J. Climate, **15**, 3096-3103.

Balas, N., Nicholson, S.E., & Klotter, D. (2007). The relationship of rainfall variability in West Central Africa to sea-surface temperatures fluctuations. International Journal of Climatology, **27**, 1335-1349.

Beck, C., Grieser, J., & Rudolf B. (2005). A New Monthly Precipitation Climatology for the Global Land Areas for the Period 1951 to 2000. Climate Status Report, pp. 181 - 190, German Weather Service, Offenbach, Germany.

Brown, M.E., & de Beurs, K. (2008). Evaluation of multi-sensor semi-arid crop season parameters based on NDVI and rainfall. Remote Sensing of Environment, **112**, 2261-2271.

Brown, M.E., de Beurs, K., & Vrieling, A. (2010). The response of African land surface phenology to large scale climate oscillations. Remote Sensing of Environment, **114**, 2286-2296.

Camberlin, P. (1995). June–September rainfall in north-eastern Africa and atmospheric signals over the tropics: A zonal perspective. Int. J. Climatol.,**15,** 773–783.

Camberlin, P., Janicot, S., & Poccard, I. (2001). Seasonality and atmospheric dynamics of the teleconnection between African rainfall and tropical sea-surface temperature: Atlantic vs

ENSO. Int. Journal of Climatology, **21**, 973-1005.

Camberlin, P., & Philippon, N. (2002). The East African March–May rainy season: associated atmospheric dynamics and predictability over the 1968–97 period. Journal of Climate, 15, 1002-1019.

Camberlin, P., Martiny, N., Philippon, N., & Richard, Y. (2007). Determinants of the interannual relationships between remote sensed photosynthetic activity and rainfall in tropical Africa. Remote Sensing of Environment, **106**, 2, 199-216.

Chen, D., Cane, M.A., Kaplan, A., Zebiak, S.E., & Huang, D. (2004). Predictability of El Niño over the past 148 years. Nature, **428**, 733-736.

Couralet, C., Sterck, F.J., Sass-Klaassen, U., Van Acker, J., & Beeckman, H. (2010). Species-specific growth responses to climate variations in understory trees of a Central African rain forest. Biotropica, **42,** 503-511.

Crétat, J., Richard, Y., Rouault, M., Reason, C.J.C., & Fauchereau, N. (2010). Recurrent daily rainfall patterns over South Africa and associated dynamics during the core of the austral summer. International Journal of Climatology, DOI: 10.1002/joc.2266.

Dai, A., & Wigley, T.M.L. (2000). Global patterns of ENSO-induced precipitation. Geophysical Research Letters, **27**, 1283-1286.

Davenport, M.L., & Nicholson, S. (1993). On the relation between rainfall and the Normalized Difference Vegetation Index for diverse vegetation types in East Africa. International Journal of Remote Sensing, **14**, 2369-2389.

Dinku, T., Ceccato, P., Grover-Kopec, E., Lemma, M., Connor, S.J., & Ropelewski, C.F. (2007). Validation of satellite rainfall products over East Africa's complex topography. International Journal of Remote Sensing, **28**, 1503-1526.

Esler, K.J., & Rundel, P.W. (1999). Comparative patterns of phenology and growth form diversity in two winter rainfall deserts: the Succulent Karoo and Mojave Desert ecosystems. Plant

Ecology, **142**, 97–104.

Fauchereau, N., Pohl, B., Reason, C.J.C., Rouault, M., & Richard, Y. (2009). Recurrent daily OLR patterns in the Southern Africa/Southwest Indian Ocean region, implications for South African rainfall and teleconnections. Climate Dynamics, **32**, 575-591.

Fontaine, B., Gaetani, M., Ullmann, A., & Roucou, P. (2011). Time evolution of observed July-September SST-Sahel climate teleconnection with removed quasi-global effect (1900-2008). Journal of Geophysical Research Atmospheres, **116,** D04105.

Fox, S.C., Hoffman, M.T., & Hoare, D. (2005). The Phenological pattern of vegetation in Namaqualand, South Africa and its climatic correlates using NOAA_AVHRR NDVI Data. South African Geographical Journal, **87**, 85-94.

Graham, E.A., Mulkey, S.S., Kitajima, K., Philipps, N.G., Wright, S.J. (2003). Cloud cover limits net CO2 uptake and growth of a rainforest tree during tropical rainy seasons. PNAS, 100, 572-576.

Giorgi, F., & Lionello, P. (2008). Climate change projections for the Mediterranean region. Global and Planetary Change, **63**, 90-104.

Gissila, T., Black, E., Grimes, D.I.F., & Slingo, J.M. (2004). Seasonal forecasting of the Ethiopian summer rains. International Journal of Climatology, **24**, 1345–1358.

Hoare, D., & Frost, P. (2009). Phenological description of natural vegetation in southern Africa using remotely-sensed vegetation data. Applied Vegetation Science, DOI: 10.1111/j.1654-109X.2004.tb00591.x.

Huete, A.R., Didan, K., Miura., T., Rodriguez, E.P., Gao, X., & Ferreira, L.G. (2002). Overview of the radiometric and biophysical performance of the MODIS vegetation indices. Remote Sensing of Environment, **83**, 195–213.

Huete, A.R., Didan, K., Shimabukuro, Y.E., Ratana, P., Saleska, S.R., Hutyra, L.R., Yang, W., Nemani, R.R., & Myneni, R. (2006). Amazon rainforests green-up with sunlight in dry season. Geophys. Res. Lett., **33**, L06405, doi:10.1029/2005GL025583.

Hutchinson, P. (1992). The Southern Oscillation and prediction of “Der” season rainfall in Somalia. Journal of Climate, 5, 525-531.

Indeje, M., Semazzi, F.H.M., & Ogallo, L.J. (2000). ENSO signals in East African rainfall seasons. Int. Journal of Climatology, 20, 19-46.

Janicot, S., Moron, V., Fontaine, B. (1996). Sahel droughts and ENSO dynamics. Geophys. Res. Lett., 23, 515–518, doi:10.1029/96GL00246.

Janicot, S., Trzaska, S., & Poccard, I. (2001). Summer Sahel-ENSO teleconnection and decadal time scale SST variations. Clim. Dyn., 18, 303-320.

Kao, H.Y., & Yu, J.Y. (2009). Contrasting Eastern-Pacific and Central-Pacific Types of ENSO. J. Climate, 22, 615–632.

Klein, D., & Röhrig, J. (2006). How does vegetation respond to rainfall variability in a semi-humid West African in comparison to a semiarid East African environment? In: Proceedings of Second Workshop of the EARSeL SIG on Remote Sensing of Land Use & Land Cover: Application and Development. Bonn, 28–30 September. (M. Braun, ed.) 149–156.

Knippertz, P., Ulbrich, U., Marques, F., & Corte-Real, J. (2003). Decadal changes in the link between El Nino and springtime North Atlantic oscillation and European-North African rainfall. International Journal of Climatology, **23**, 1293-1311.

Kogan, F.N. (2000). Satellite-observed sensitivity of world land ecosystems to El Niño/La Niña. Remote Sensing of Environment, 74, 445-462.

Lamb, P.J., & Peppler, R.A. (1991). West Africa. In Teleconnections Linking Worldwide Climate Anomalies, Glantz MH, Katz RW, Nicholls N (eds). Cambridge University Press: Cambridge, 546p.

Larkin, N.K., & Harrison, D. E. (2002) ENSO Warm (El Niño) and Cold (La Niña) Event Life Cycles: Ocean Surface Anomaly Patterns, Their Symmetries, Asymmetries, and Implications.

J. Climate, **15**, 1118–1140.

Latif, M., Anderson, D., Barnett, T., Cane, M., Kleeman, R., Leetmaa, A., O'Brien, J., Rosati, A., Schneider, E. (1998). A review of the predictability and prediction of ENSO. Journal of Geophysical Research, **103**, 14375-14393.

Linthicum, K.J., Anyamba, A., Tucker, C.J., Kelley, P.W., Myers, M.F., & Peters, C.J. (1999). Climate and satellite indicators to forecast Rift Valley fever epidemics in Kenya. Science, 285, 397-400.

Los, S.O., Collatz, S.J., Bounoua, L., Sellers, P.J., & Tucker, C.J. (2001). Global Interannual Variations in Sea Surface Temperature and Land Surface Vegetation, Air Temperature, and Precipitation. Journal of Climate, 14, 1535-1549.

Lyon, B., Mason, S.J. (2007). The 1997–98 Summer Rainfall Season in Southern Africa. Part I: Observations. J. Climate, **20**, 5134–5148.

McCollum, J.R., Gruber, A., Ba, M.B. (2000). Discrepancy between gauges and satellite estimates of rainfall in Equatorial Africa. J. Appl. Meteor., **39**, 666–679.

McKellar, N.C., Hewitson, B.C., & Tadross, M.A. (2007). Namaqualand's climate: recent historical scenarios, Journal of Arid Environments. **70**, 604-614.

Malhi, Y., & Wright, J. (2004). Spatial patterns and recent trends in the climate of tropical rainforest regions. Phil. Trans. R. Soc. Lond. B, **359**, 311-329.

Malo, A.R., & Nicholson, S. (1990). A study of rainfall and vegetation dynamics in the African Sahel using normalized difference vegetation index. Journal of Arid Environments, **19,** 1-24.

Mapande, A.T., & Reason, C.J.C. (2005) Interannual rainfall variability over Western Tanzania, International Journal of Climatology, DOI: 10.1002/joc.1193.

Mariotti, A., Zeng, N., & Lau, K.M. (2002). Euro-Mediterranean rainfall and ENSO — a seasonally varying relationship. Geophysical Research Letters, **29**, 591–594.

Martiny, N., Camberlin, P., Richard, Y., & Philippon, N. (2006). Compared regimes of NDVI and rainfall in semi-arid regions of Africa. International Journal of Remote Sensing, **27**, 5201-5223.

Martiny, N., Philippon, N., Richard, Y., Camberlin, P., & Reason, C.J.C. (2009). Predictability of NDVI in semi-arid African regions. Theoretical and Applied Climatology, doi. 10.1007/sOO704-009-0223-9.

Mason, S.J. (2001). El Niño, climate change, and Southern African climate. Environmetrics, 12, 327-345.

Mayaux, P., Bartholomé, E., Fritz, S., Beward, A. (2004). A new land-cover map of Africa for the year 2000. Journal of Biogeography, **31**: 861–877.

Meyers, N., Mittermeier, R.A., Mittermeier, C.G., da Fonseca, G.A.B., & Kent, J., (2000). Biodiversity hotspots for conservation priorities. Nature, **403**: 853-858.

Myneni, R.B., Los, S.O., & Tucker, C.J. (1996). Satellite-based identification of linked vegetation index and sea surface temperature anomaly areas from 1982-1990 for Africa, Australia and South America. Geophysical Research Letters, 23, 729-732.

Misra, V. (2010). Interaction of interannual and diurnal variations over equatorial Africa. J. Geophys. Res., **115**, D01111, doi:10.1029/2009JD012512.

Mohino, E.B., Rodriguez-Fonseca, B., Mechoso, C.R., Gervois, S., Ruti, P., & Chauvin, F. (2011). West Africa Monsoon response to tropical Pacific sae surface anomalies. Journal of Climate, submitted.

Mutai, C.C., & Ward, N.M. (2000). East African Rainfall and the Tropical Circulation/Convection on Intraseasonal to Interannual Timescales. J. Climate, **13**, 3915–3939.

Newman, M., Shin, S.I., & Alexander, M.A. (2011). Natural variation in ENSO flavors. Geophys. Res. Lett., **38**, L14705, doi:10.1029/2011GL047658.

Nicholson, S.E., Davenport, M.L., & Malo, A.R. (1990). A comparison of the vegetation response to rainfall in the Sahel and East Africa, using normalized difference vegetation index from

NOAA AVHRR. Climatic change, 17, 209-241.

Nicholson, S.E., & Kim, J. (1997). The relationship of the El Niño-Southern Oscillation to the African rainfall. International Journal of Climatology, **17**, 117-135.

Nicholson, S.E., & Grist, J.P. (2003). The seasonal evolution of the atmospheric circulation over West Africa and equatorial Africa. Journal of Climate, **16**, 1013-1030.

Nicholson, S.E. and Coauthors (2003). Validation of TRMM and Other Rainfall Estimates with a High-Density Gauge Dataset for West Africa. Part II: Validation of TRMM Rainfall Products. J. Appl. Meteor., **42**, 1355–1368.

Ogallo, L.J. (1988). Relationships between seasonal rainfall in East Africa and the Southern Oscillation. J. Climatol., 8, 31–43.

Pau, S., Okin, G.S., Gillepsie, T.W. (2010). Asynchronous response of tropical forest leaf phenology to seasonal and El Niño driven drought. Plos ONE, 5, e11325.

Philippon, N., Jarlan, L., Martiny, N., Camberlin, P., & Mougin, E. (2007). Characterization of the interannual and intraseasonal variability of West African vegetation between 1982-2002 by means of NOAA-AVHRR NDVI data. Journal of Climate, **20**, 1202-1218.

Philippon, N., Rouault, M., Richard, Y., & Favre A. (2011). The influence of ENSO on South African winter rainfall. International Journal of Climatology, DOI: 10.1002/joc.3403.

Phillips, J., & McIntyre, B. (2000). ENSO and interannual rainfall variability in Uganda: implications for agricultural management. Int. J. Climatol., 20: 171-182.

Pinzon, J., Brown, M.E., & Tucker, C.J. (2004). Satellite time series correction of orbital drift artifacts using empirical mode decomposition. Hilbert-Huang Transform: Introduction and Applications. N. Huang: Chapter 10, Part II. Applications.

Poccard, I., Janicot, S., & Camberlin, P. (2000). Comparison of rainfall structures between NCEP/NCAR reanalyses and observed data over tropical Africa. Climate Dynamics, 16, 897-915.

Pohl, B., Fauchereau, N., Richard, Y., Rouault, M., & Reason, C.J.C. (2009). Interactions between synoptic, intraseasonal and interannual convective variability over Southern Africa. Climate Dynamics, 33, 1033-1050.

Propastin, P., Fosto, L., & Kappas, M. (2010). Assessment of vegetation vulnerability to ENSO warm events over Africa. International Journal of Applied Earth Observation and Geoinformation, DOI: 10.1016/j.jag.2009.10.007.

Ren, H.L., Jin, F.F. (2011). Niño indices for two types of ENSO. Geophys. Res. Lett., 38, L04704, doi:10.1029/2010GL046031.

Richard, Y., Trzaska, S., Roucou, P., & Rouault, M. (2000). Modification of the Southern African rainfall variability / ENSO relationship since the late 1960s. Climate Dynamics, 16, 883-895.

Richard, Y., Camberlin, P., Fauchereau, N., & Mulenga, H. (2002). Cohérence intra-saisonnière de la variabilité pluviométrique en Afrique du Sud. Espace Géographique, 2, 63-72.

Rodriguez-Fonseca, B., Janicot, S., Mohino, E., Losada, T., Bader, J., Caminade, C., Chauvin, F., Fontaine, B., Garcia-Serrano, J., Gervois, S., Joly, M., Polo, I., Ruti, P., Roucou, P., & Voldoire, A. (2011). Interannual and decadal SST-forced responses of the West African monsoon. Atmos. Science Lett., **12**, 67-74.

Rouault, M. & Richard, Y. (2003). Intensity and spatial extension of drought in South Africa at different time scales. Water SA, **29**, 489-500.

Rowell, D.P. (2001). Teleconnections between the tropical Pacific and the Sahel. Quarterly Journal of the Royal Meteorological Society, **127**, 1683–1706.

Rudolf, B., & Schneider, U. (2005). Calculation of Gridded Precipitation Data for the Global Land-Surface using in-situ Gauge Observations. Proceedings of the 2nd Workshop of the International Precipitation Working Group IPWG, Monterey October 2004, EUMETSAT, ISBN 92-9110-070-6, ISSN 1727-432X, 231-247.

Segele, Z.T., Lamb, P.J., & Leslie, L.M. (2008). Large-scale atmospheric circulation and global sea surface temperature associations with Horn of Africa June–September rainfall. Int. J. Climatol., 29, 1075–1100

Smith, T.M., Reynolds, R.W., Peterson, T.C., & Lawrimore, J. (2008). Improvements to NOAA's Historical Merged Land-Ocean Surface Temperature Analysis (1880-2006). J. Clim., **21,** 2283-2296.

Heyden, F., & Lewis, O.A.M. (1992). Plant structure and function. In: Cowling RM (ed). "The ecology of Fynbos: nutrients, fire and diversity", 226-240.

Thornton, P.K., Jones, P.G., Owiyo, T., Kruska, R.L., Herrero, M., Kristjanson, P., Notenbaert, A., Bekela, N., Omolo, A., with contributions from Orindi, V., Otiende, B., Ochieng, A., Bhadwal, S., Anantram, K., Nair, S., Kumar, V., Kulkar, U. (2006). Mapping climate vulnerability and poverty in Africa. Report to the Department for International Development, ILRI, PO Box 30709, Nairobi 00100, Kenya, 171p.

Tucker, C.J., Pinzón, J.E., Brown, M.E., Slayback, D., Pak, E.W., Mahoney, R., Vermote, E., El Saleous, N. (2005). An Extended AVHRR 8-km NDVI Data Set Compatible with MODIS and SPOT Vegetation NDVI Data. International Journal of Remote Sensing, **26**, 4485-4498.

Verdin, J., Funk, C., Klaver, R., Roberts, D. (1999). Exploring the correlation between South African NDVI and Pacific sea-surface temperatures: results for the 1998 maize growing season. International Journal of Remote Sensing, **20**, 2117-2124.

Vrieling, A., de Beurs, K.M., Brown, M.E. (2011). Phenological characterization and variability of african farming systems with NDVI time series. Climatic Change, DOI 10.1007/s10584-011-0049-1.

Ward, M.N. (1998). diagnosis and short-lead time prediction of summer rainfall in tropical north Africa at interannual and multidecadal timescales. Journal of Climate, **11**, 3167-3191.

Williams, C.A., & Hanan, N.P. (2011). ENSO and IOD teleconnections for African ecosystems: Evidence of destructive interference between climate oscillations. Biogeosciences, **8**, 27-40.

Zhang, X., Friedl, M.A., Schaaf, C.B., Strahler, A.H., Hodges, J.C.F., Reed, B.C., & Huete, A. (2003). Monitoring vegetation phenology using MODIS. Remote Sensing of Environment, **84**, 471-475.

Zhang, P., Anderson, B., Barlow, M., Tan, B., & Myneni, R.B. (2004). Climate-related vegetation characteristics derived from Moderate Resolution Imaging Spectroradiometer (MODIS) leaf area index and normalized difference vegetation index. J. Geophys. Res., **109**, D20105, doi:10.1029/2004JD004720.

Zhang, X., Friedl, M.A., Schaaf, C.B., Strahler, A.H., & Liu, Z. (2005). Monitoring the response of vegetation phenology to precipitation in Africa by coupling MODIS and TRMM instruments. J. Geophys. Res., **110**, D12103, doi:10.1029/2004JD005263.

Figures captions

Figure 1a: month of the vegetative season onset (average over the 27 years) defined as the month when NDVI reaches up to the annual mean level.

Figure 1b: same as figure 1a but for the end of the vegetative season, defined as the month when NDVI reaches down to the annual mean level.Figure 2a: July to December correlation maps between 3-month rainfall amounts and monthly NDVI with one-month lag (i.e. April-May-June rainfall amount correlated to July NDVI). Pixels/months which are not falling within the vegetative season are masked. The black lines in the colorbar denote the 95% significance level (|0.3809|).

Figure 2b: same as Figure 2a but for January to June.

Figure 3a: mean annual rainfall amount from GPCC over the period 1981-2007.

Figure 3b: mean number of stations per grid point over the period 1981-2007.

Figure 4: Vegetation cover for Africa issued from the Global Land Cover 2000 (GLC2000) project.

Figure 5a: July to December correlation maps between 3-month NINO3.4 and monthly NDVI with one-month lag (i.e. April-May-June NINO3.4 correlated to July NDVI). Pixels/months which are not falling within the vegetative season are masked. The black lines in the colorbar denote the 95% significance level (|0.3809|).

Figure 5b: same as figure 5a but for January to June.

Figure 6a: July to December synthetic maps of the correlations between NINO3.4 and NDVI and rainfall (e.g. April-May-June NINO3.4 is correlated to April-May-June rainfall and July NDVI, see text for an explanation of the construction of the maps). Pixels/months which are not falling within the vegetative season are masked.

Figure 6b: same as figure 6a but for January to June.

Figure 7: monthly evolution of NDVI (green thick line; triangles denote the vegetative season) and NDVI-N3.4 correlations over 5 selected regions. Black thick line: correlation between a NDVI regional index and N3.4 index. Black thin solid line : mean of the pixels correlations. Black thin dashed lines: 25 and 75 percentiles of the pixels correlations.

Figure 1a

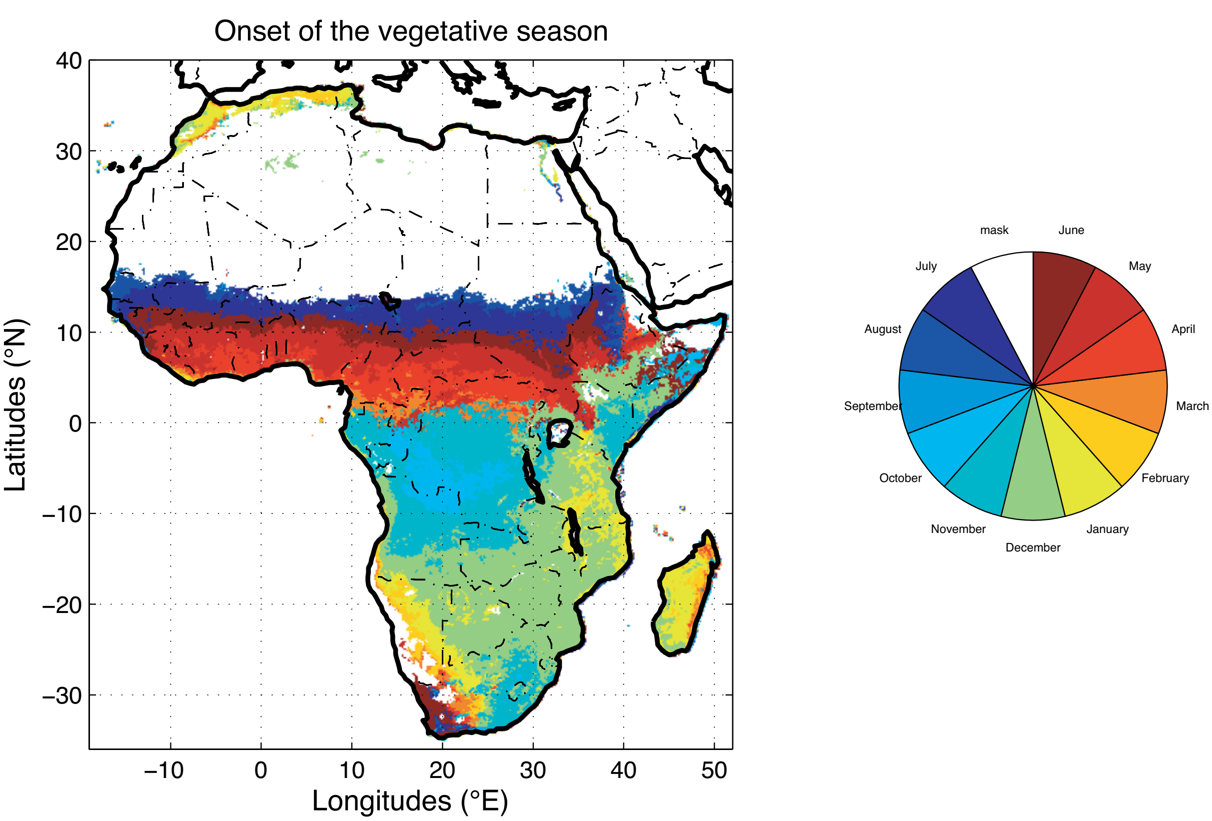

Onset of the vegetative season
40
30
20
10
0
−10
−20
−30
Latitudes (°N)
−10
0
10
20
30
40
50
Longitudes (°E)
mask
June
May
April
March
February
January
December
November
October
September
August
July

Figure 1b

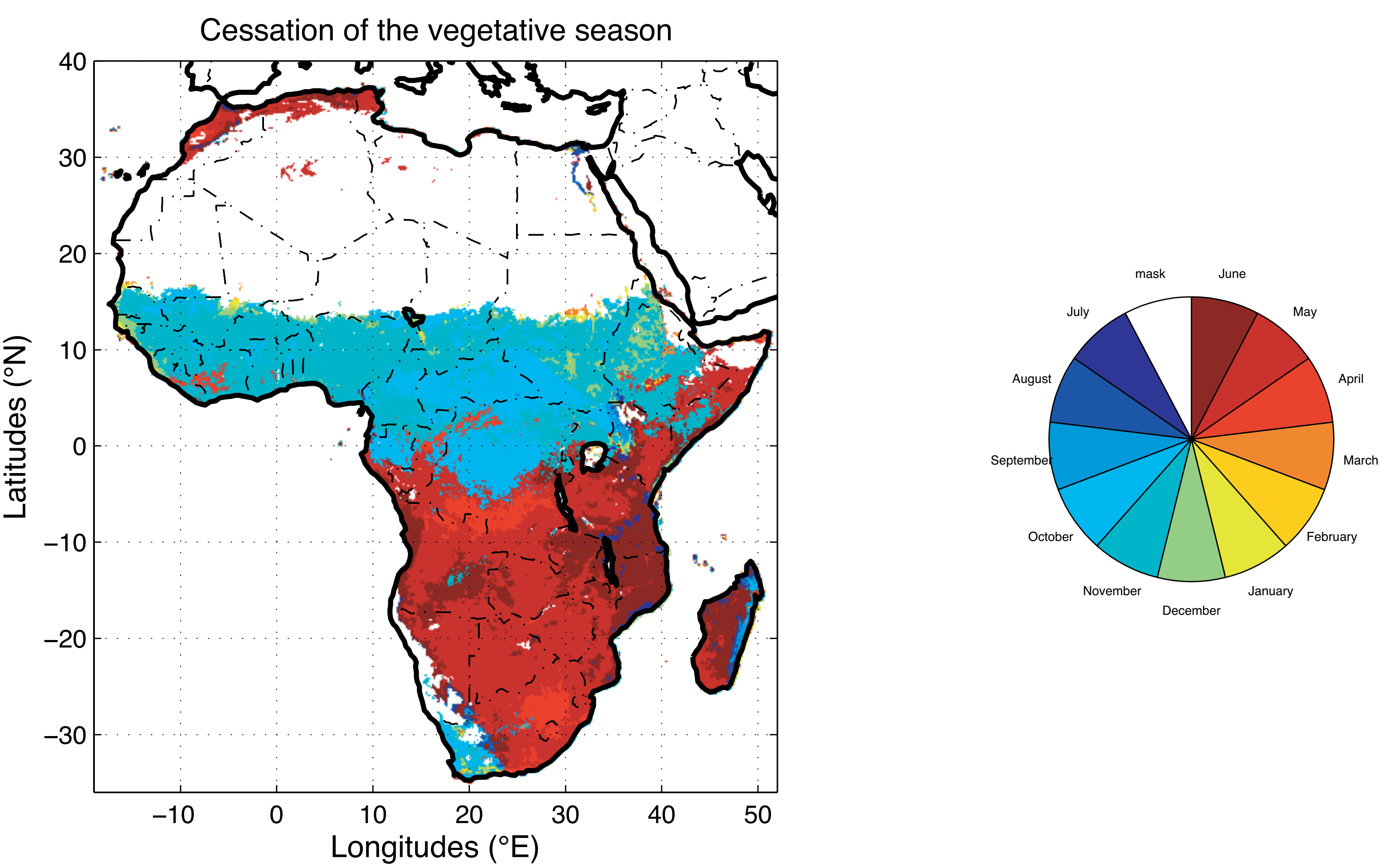

Cessation of the vegetative season
Latitudes (°N)
Longitudes (°E)
40
30
20
10
0
−10
−20
−30
−10
0
10
20
30
40
50
mask
June
May
April
March
February
January
December
November
October
September
August
July

Figure 2a

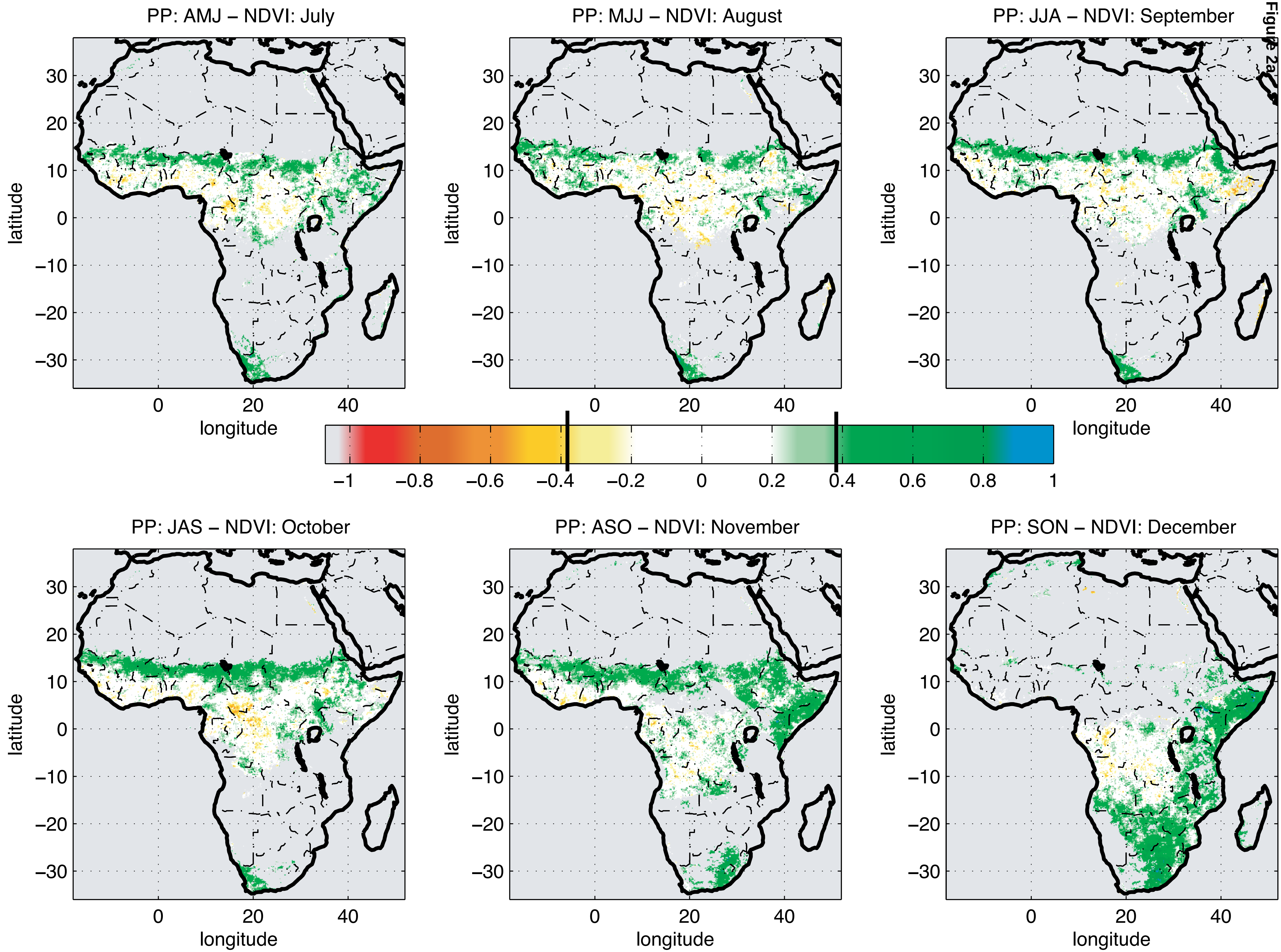
PP: AMJ – NDVI: July
PP: MJJ – NDVI: August
PP: JJA – NDVI: September
PP: JAS – NDVI: October
PP: ASO – NDVI: November
PP: SON – NDVI: December
latitude
longitude
30
20
10
0
−10
−20
−30
0
20
40
−1
−0.8
−0.6
−0.4
−0.2
0
0.2
0.4
0.6
0.8
1

Figure2b

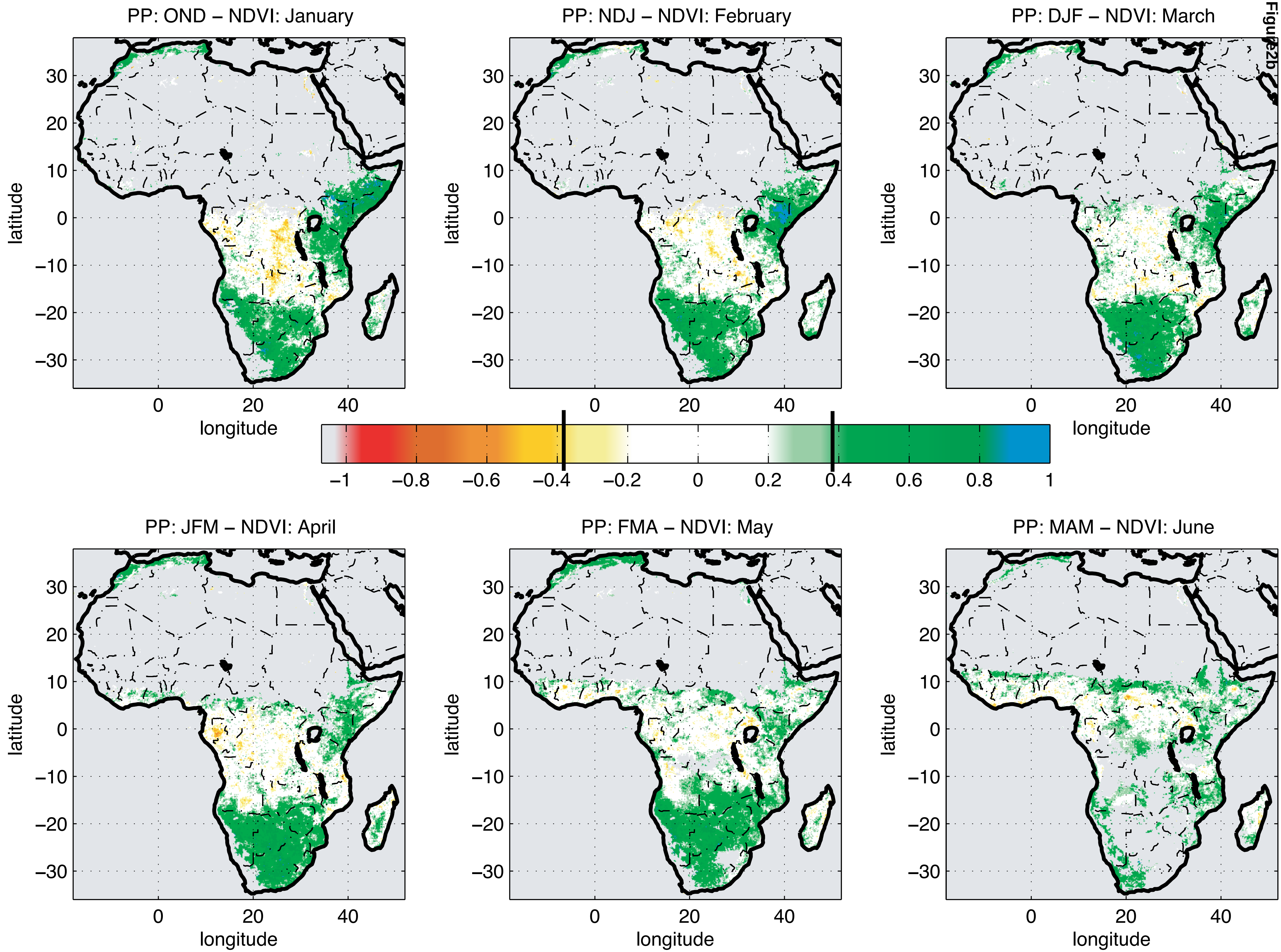

PP: OND – NDVI: January
PP: NDJ – NDVI: February
PP: DJF – NDVI: March
PP: JFM – NDVI: April
PP: FMA – NDVI: May
PP: MAM – NDVI: June
latitude
longitude
−1
−0.8
−0.6
−0.4
−0.2
0
0.2
0.4
0.6
0.8
1

Figure 3a

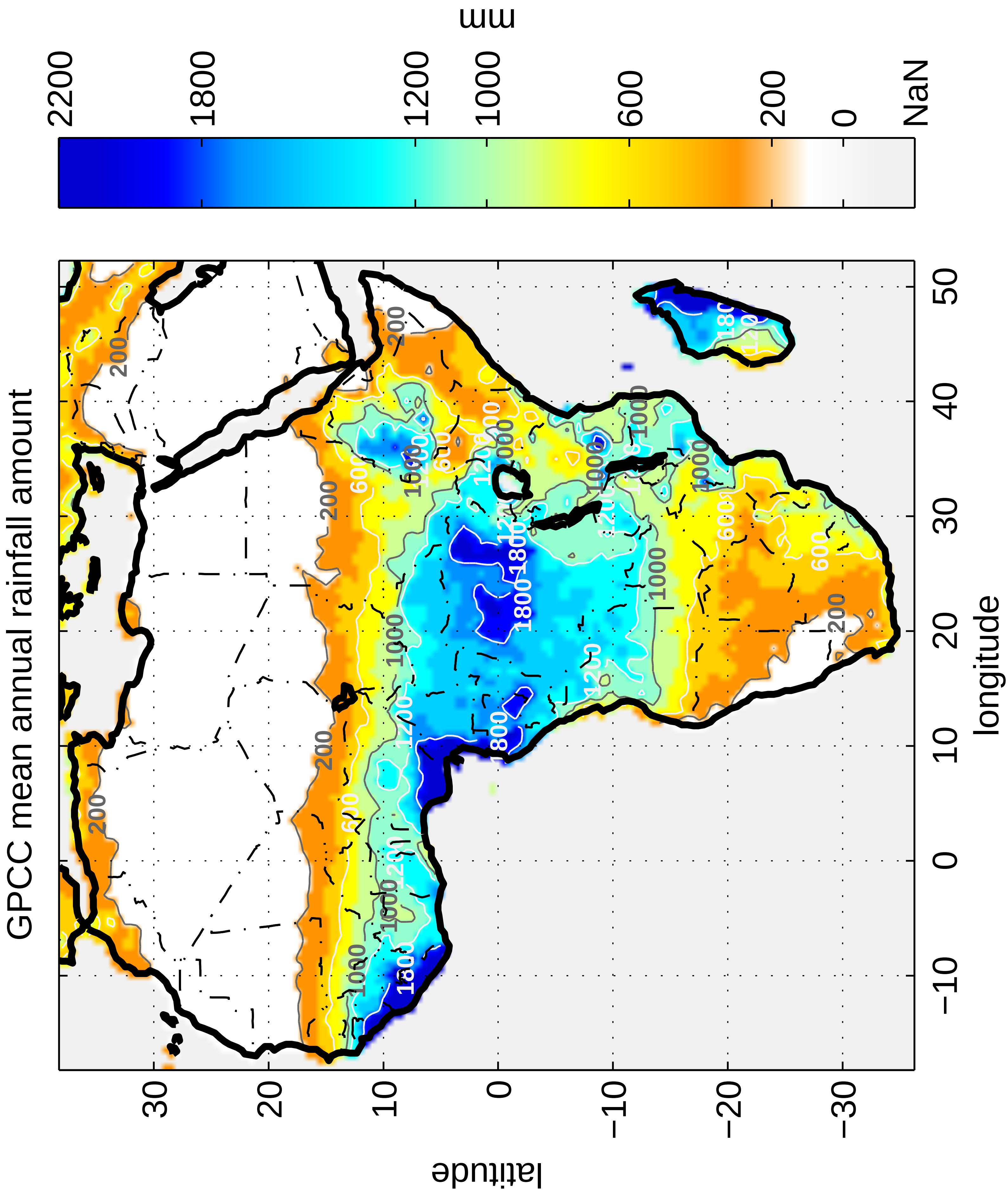
GPCC mean annual rainfall amount
mm
2200
1800
1200
1000
600
200
0
NaN
latitude
longitude
30
20
10
0
−10
−20
−30
50
40

Figure 3b

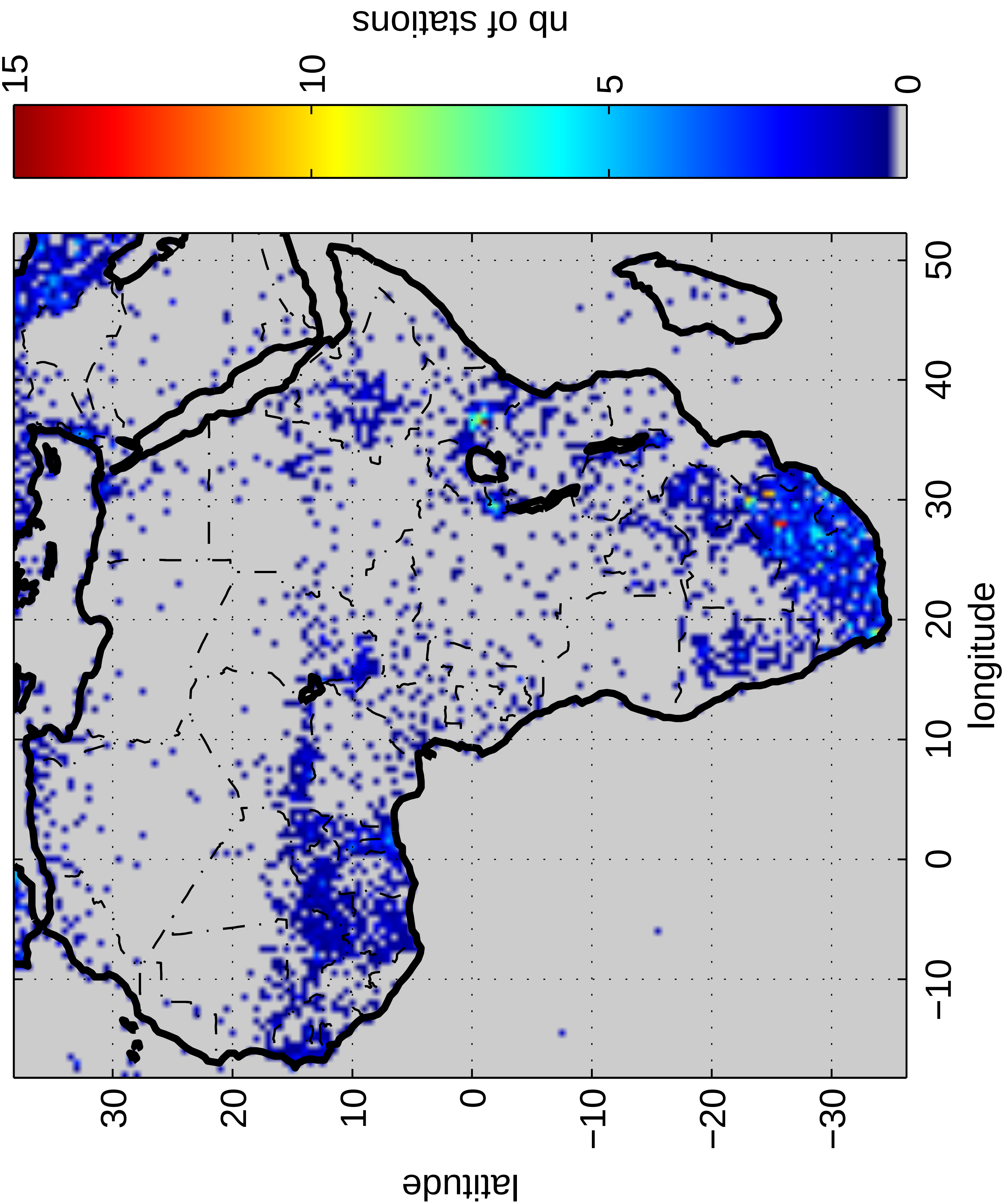
nb of stations
0
5
10
15
latitude
30
20
10
0
−10
−20
−30
longitude
−10
0
10
20
30
40
50

Figure 4

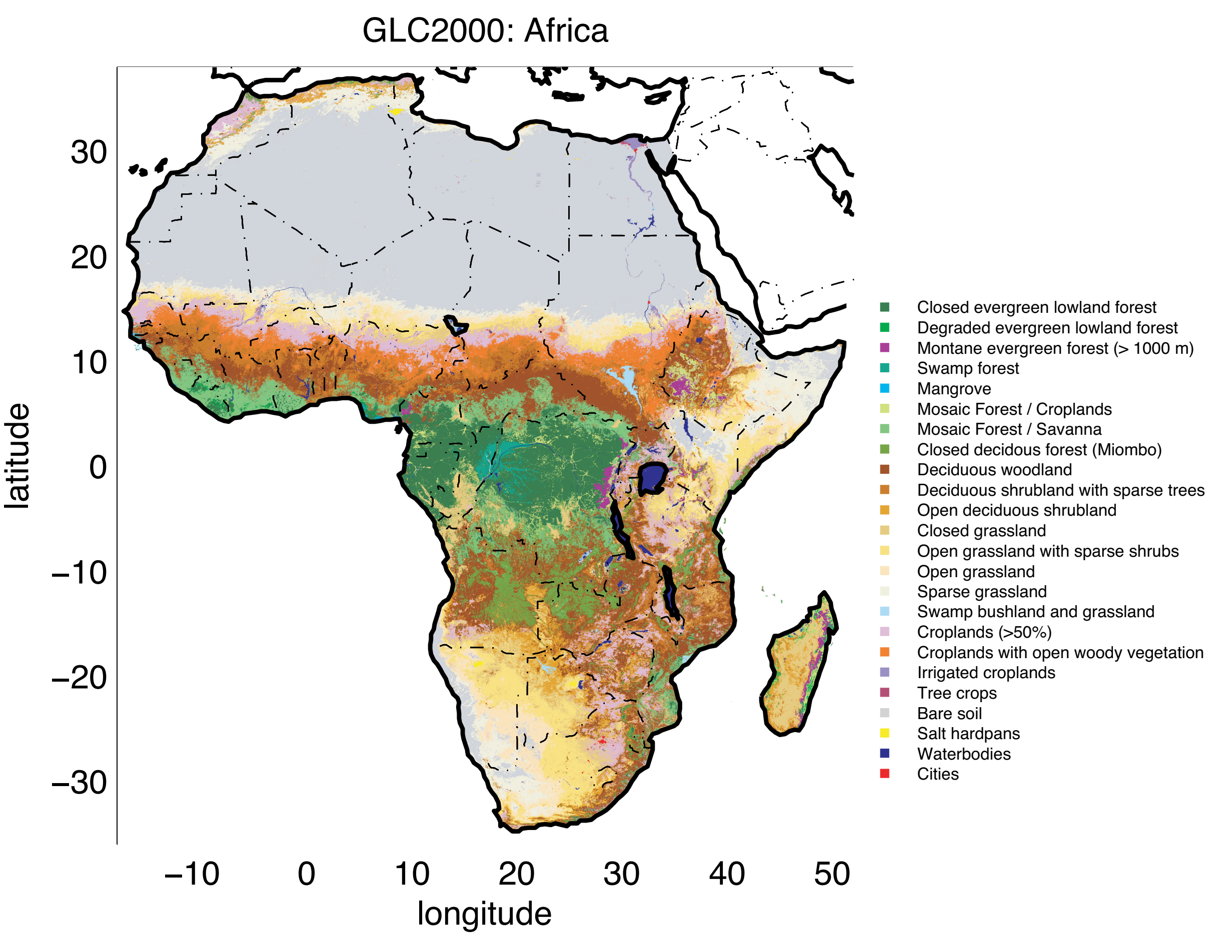
GLC2000: Africa
30
20
10
0
−10
−20
−30
latitude
−10
0
10
20
30
40
50
longitude
Closed evergreen lowland forest
Degraded evergreen lowland forest
Montane evergreen forest (> 1000 m)
Swamp forest
Mangrove
Mosaic Forest / Croplands
Mosaic Forest / Savanna
Closed decidous forest (Miombo)
Deciduous woodland
Deciduous shrubland with sparse trees
Open deciduous shrubland
Closed grassland
Open grassland with sparse shrubs
Open grassland
Sparse grassland
Swamp bushland and grassland
Croplands (>50%)
Croplands with open woody vegetation
Irrigated croplands
Tree crops
Bare soil
Salt hardpans
Waterbodies
Cities

Figure 5

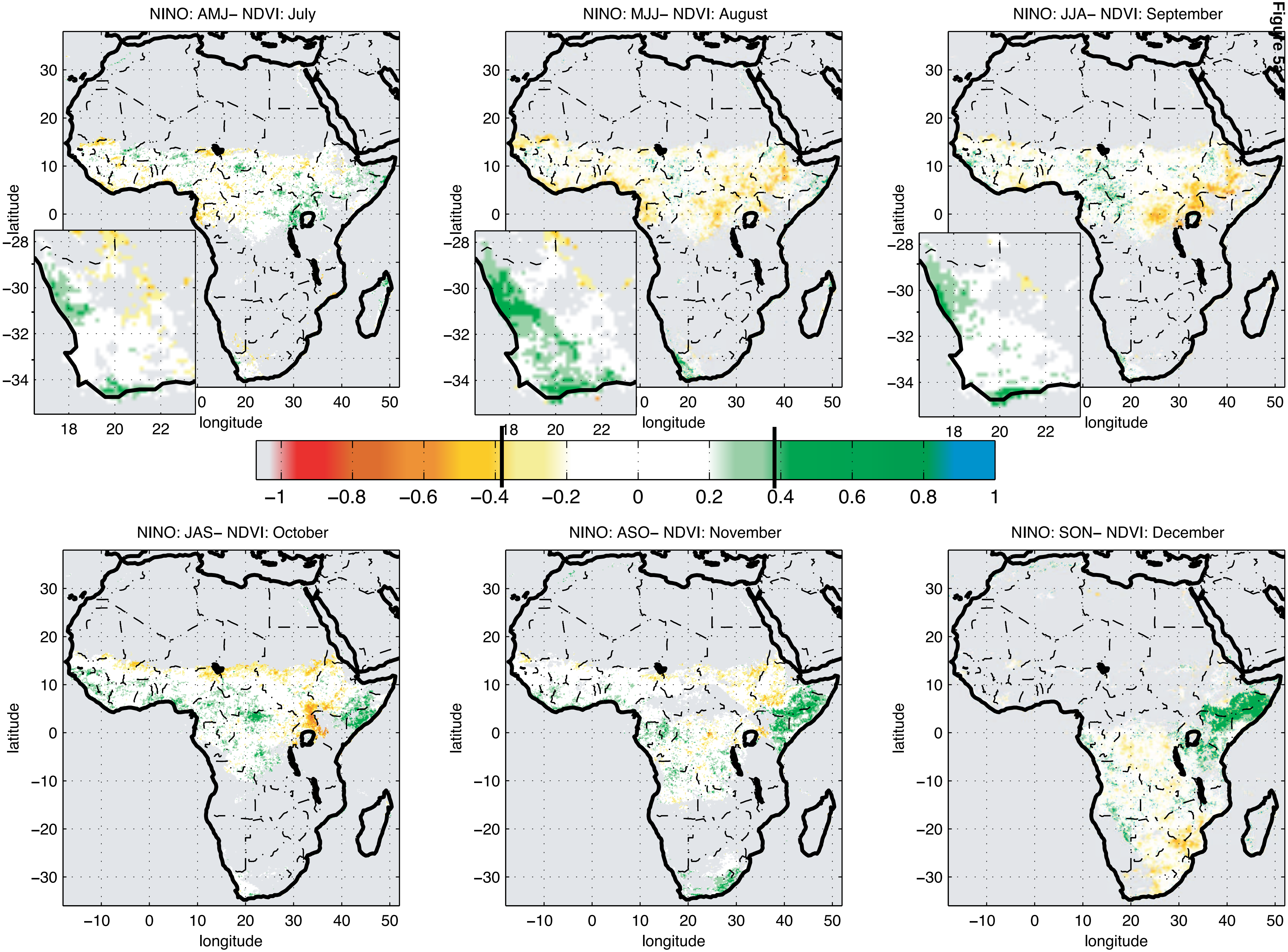

NINO: AMJ– NDVI: July
NINO: MJJ– NDVI: August
NINO: JJA– NDVI: September
NINO: JAS– NDVI: October
NINO: ASO– NDVI: November
NINO: SON– NDVI: December
latitude
longitude
−1
−0.8
−0.6
−0.4
−0.2
0
0.2
0.4
0.6
0.8
1

Figure 5b

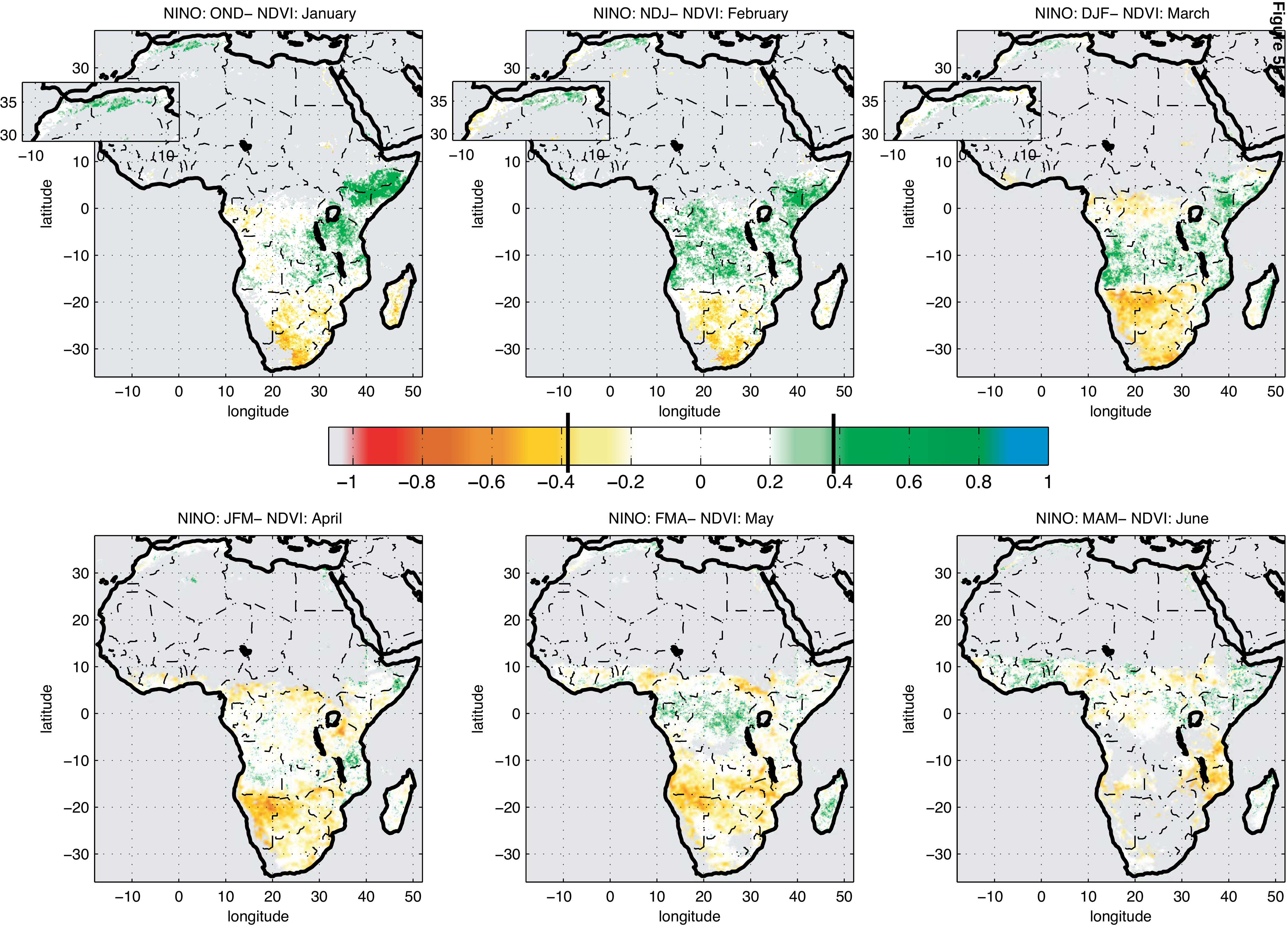
NINO: OND– NDVI: January
NINO: NDJ– NDVI: February
NINO: DJF– NDVI: March
NINO: JFM– NDVI: April
NINO: FMA– NDVI: May
NINO: MAM– NDVI: June
latitude
longitude
−1 −0.8 −0.6 −0.4 −0.2 0 0.2 0.4 0.6 0.8 1

Figure 6

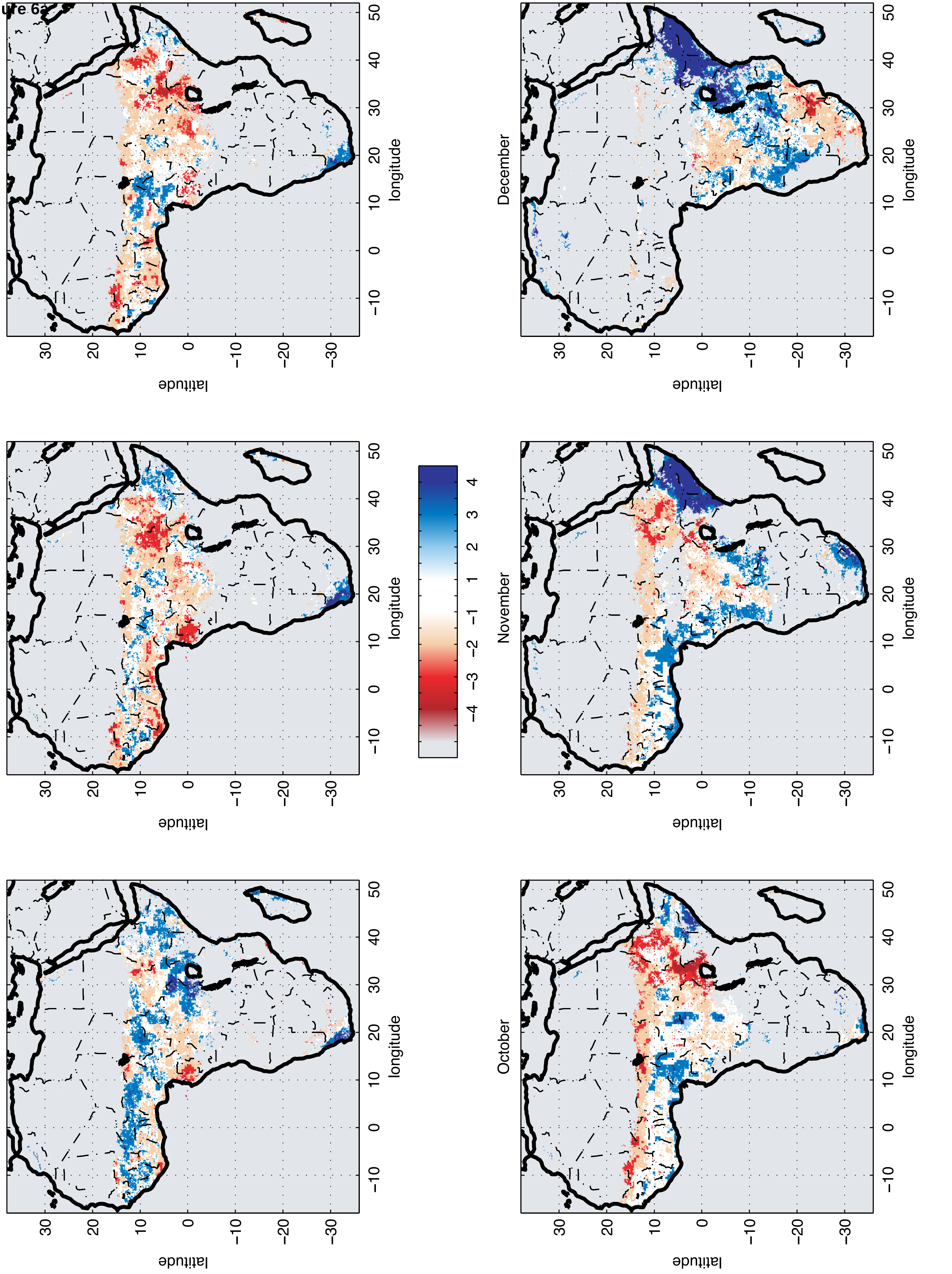

July
August
September
October
November
December
latitude
longitude

Figure 6b

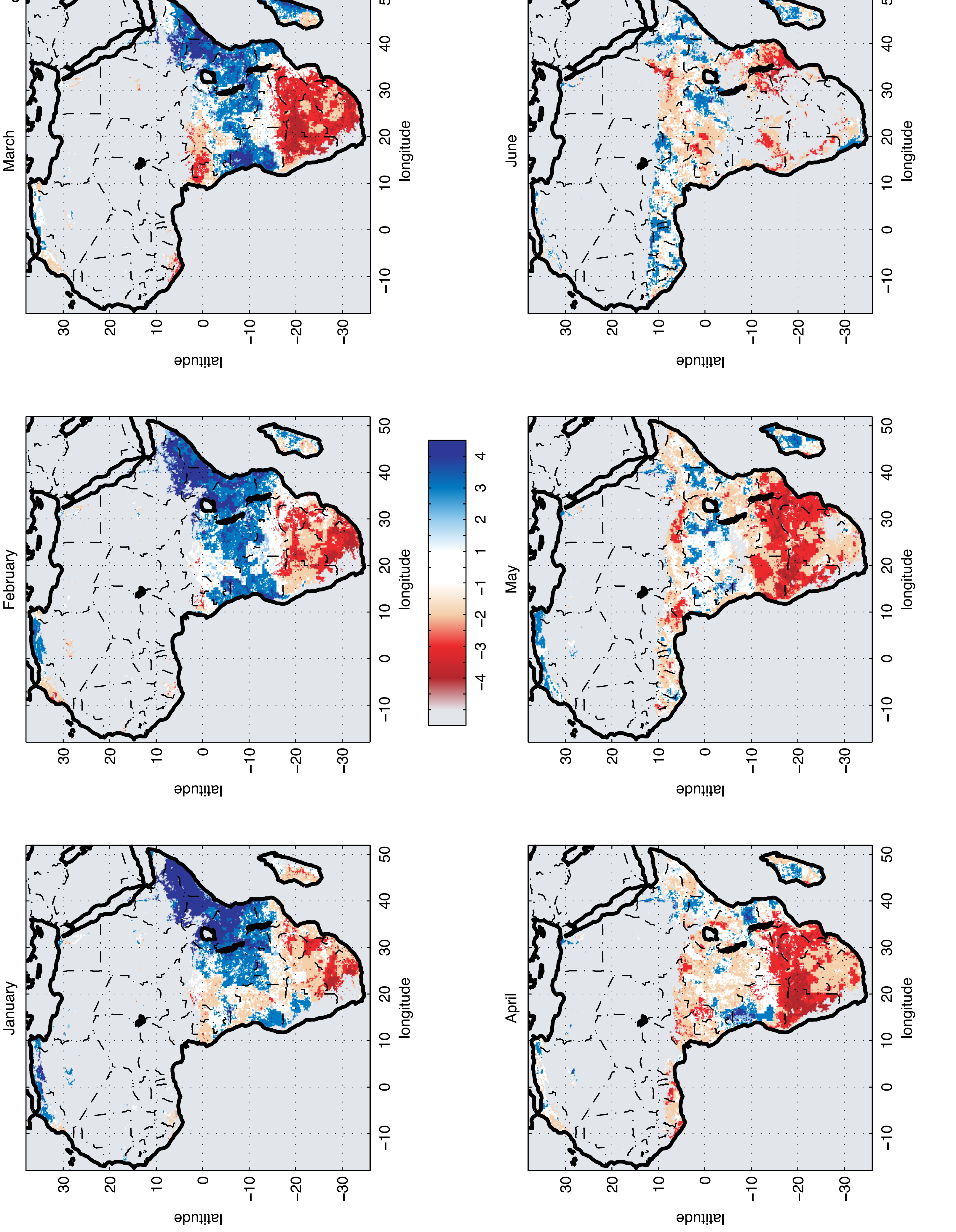

January
February
March
April
May
June
latitude
longitude
4
3
2
1
−1
−2
−3
−4

Figure 7

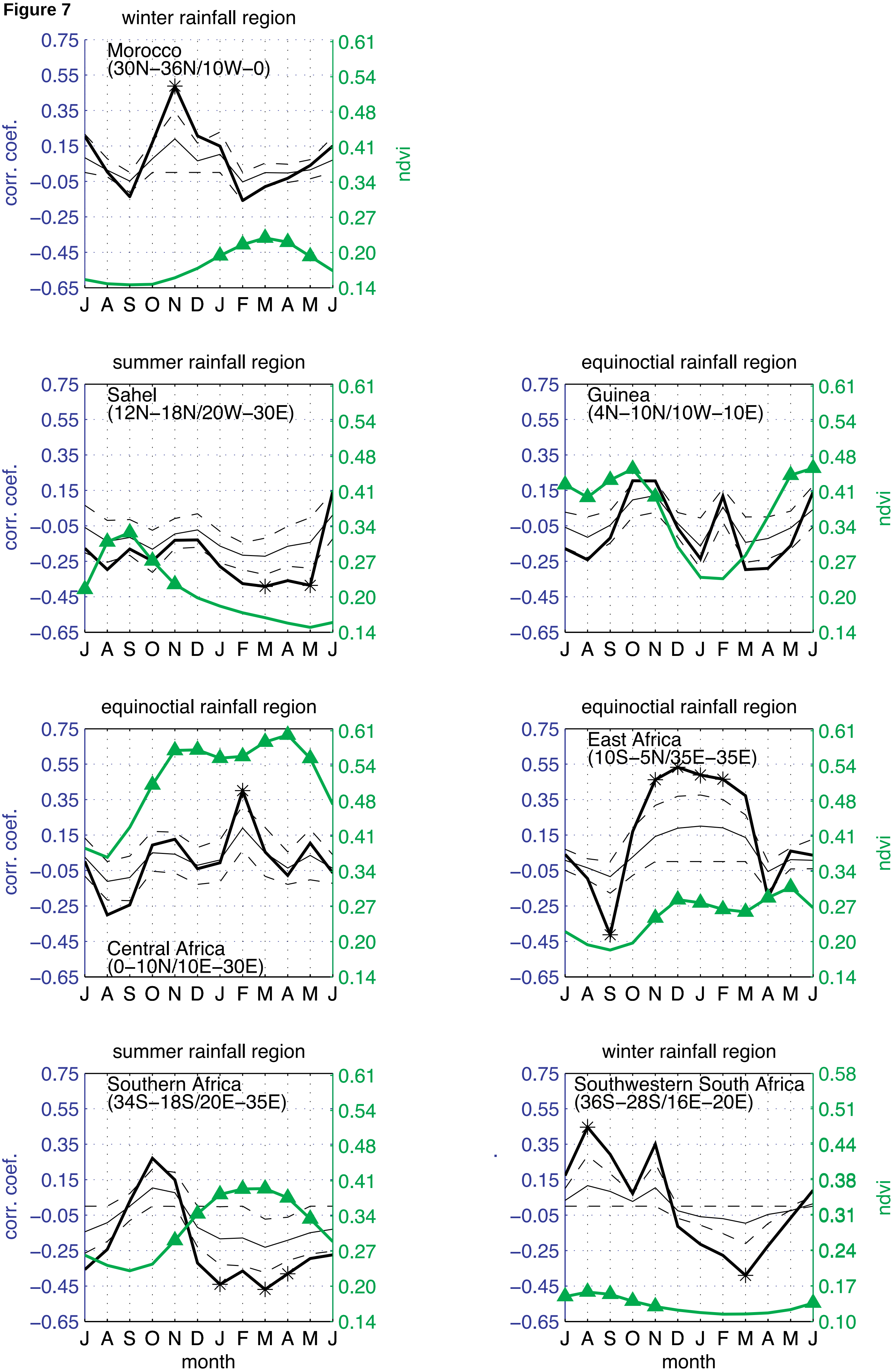
winter rainfall region
Morocco
(30N–36N/10W–0)
summer rainfall region
Sahel
(12N–18N/20W–30E)
equinoctial rainfall region
Guinea
(4N–10N/10W–10E)
equinoctial rainfall region
Central Africa
(0–10N/10E–30E)
equinoctial rainfall region
East Africa
(10S–5N/35E–35E)
summer rainfall region
Southern Africa
(34S–18S/20E–35E)
winter rainfall region
Southwestern South Africa
(36S–28S/16E–20E)
corr. coef.
ndvi
month
J A S O N D J F M A M J